Marked decrease of the near surface snow density retrieved by AMSR-E satellite at Dome C, Antarctica, between 2002 and 2011

Nicolas Champollion[1,*], Ghislain Picard[1], Laurent Arnaud[1], Éric Lefebvre[1], Giovanni Macelloni[2], Frédérique Rémy[3], and Michel Fily[1]

[1]Univ. Grenoble Alpes, CNRS, IRD, Grenoble INP, IGE – UMR 5001, 38000 Grenoble, France,
[*]Now at the Climate Lab – University of Bremen, Celsiusstrasse 2 FVG–M2040, 28359 Bremen, Germany
[2]Institute of Applied Physics / IFAC - CNR, Via Madonna del Piano 10, 50019 Fiorentino, Italy
[3]UPS / CNRS, Laboratoire d'Étude en Géophysique et Océanographie Spatiales (LEGOS) - Observatoire Midi-Pyrénées (OMP), 18 av. Edouard Belin, 31401, Toulouse cedex 9, France

Correspondence: Champollion Nicolas
(nicolas.champollion@uni-bremen.de)

Abstract. Surface snow density is an important variable for the surface mass balance and energy budget. It evolves according to meteorological conditions, in particular snowfall, wind and temperature, but the physical processes governing atmospheric influence on snow are not fully understood. A reason is that no systematic observation is available on a continent scale. Here, we use the passive microwave observations from AMSR-E satellite to retrieve the surface snow density at Dome C in the East
5 Antarctic Plateau. The retrieval method is based on the difference of surface reflections between horizontally– and vertically–polarised brightness temperatures at 37 GHz, highlighted by the computation of the polarisation ratio, which is related to surface snow density. The relationship has been obtained with a microwave emission radiative transfer model (DMRT-ML). The retrieved density, representative of the topmost 3 centimetres of the snowpack, compares well with in situ measurements. The difference between mean in situ measurements and mean retrieved density is $26.2 \, \mathrm{kg \, m^{-3}}$, which is within typical in situ
10 measurement uncertainties. We apply the retrieval method to derive the time series over the period 2002–2011. The results show a marked and persistent pluri-annual decrease of about $10 \, \mathrm{kg \, m^{-3} \, yr^{-1}}$, in addition to atmosphere–related seasonal, weekly and daily density variations. This trend is confirmed by independent active microwave observations from ENVISAT and QuickSCAT satellites though the link to the density is more difficult to establish. However, no related pluri-annual changes in meteorological conditions has been found to explain such trend in snow density. Further work concern the extension of the
15 method at the continent scale.

Keywords: Surface Snow Density ; Antarctic Ice Sheet ; Passive & Active Microwave Remote Sensing ; Electromagnetic Modelling ; In Situ Snow Property Observations ; Retrieval Method.

1   Introduction

Snow density is an important variable relating snow thickness and mass. Close to the surface, its value is necessary to establish the surface mass balance from in situ measurements using stake, ultrasonic sensor, ground-penetrating radar, snowpit or firn cores (Eisen et al., 2008), and from satellite observations (microwave radiometer and lidar or radar altimeters, Arthern et al.,

5 2006; Flament and Rémy, 2012; McMillan et al., 2014; Palerme et al., 2014; Markus et al., 2017). It is useful for the validation of regional climate modelling (Lenaerts and van den Broeke, 2012; Fettweis et al., 2013; Vernon et al., 2013). Surface snow density is also important to study the surface energy budget (Brun et al., 2011; Favier et al., 2011; Libois et al., 2013; Freville et al., 2014), firn densification (Alley et al., 1982; Fujita et al., 2011) and air–snow exchanges (Dominé et al., 2008; France et al., 2011). Its evolution is related to the local meteorological conditions such as precipitation, wind speed and air temperature (Brun

10 et al., 2011; Champollion et al., 2013; Libois et al., 2014; Freville et al., 2014). However, their links are complex and not well known. For example, snowfall can lead to different surface density behaviours depending on initial snow conditions: over hard and dense surface snow, snowfall results in a decrease of surface snow density ; over surface hoar crystals, snowfall increases surface snow density. More complex are the interactions between the different meteorological effects. Wind often increases surface snow density (Sommer et al., 2018) and water vapour fluxes into the snowpack are regularly oriented towards the

15 atmosphere resulting in a decrease of the density near the surface. However, wind can also contribute to sublimate snow and thus change snow metamorphism (Dominé et al., 2008).

Estimating the surface snow density in Antarctica remains difficult (Eisen et al., 2008; Zwaaftink et al., 2013). It is presently not retrieved from satellite remote sensing (Groh et al., 2014), and the snow density estimates from regional climate and snowpack modelling are highly uncertain close to the surface (Brun et al., 2011; Fettweis et al., 2013). Nevertheless, Schwank

20 and Naderpour (2018) recently presented encouraging results about the retrieval of snow density from ground-based L-band radiometry. However, this method is valid only for a soil bottom layer. In addition, despite some recent progress to automatically measure the snow density in the field (Mittal et al., 2009; Gergely et al., 2010), manual measurements are more accurate, with a typical accuracy around 11% (Conger and McClung, 2009). It results in a low spatial and temporal coverage of Antarctica, especially in the East Antarctica Plateau where data are mainly acquired during traverses or close to stations (Favier et al., 2012;

25 Zwaaftink et al., 2013). Close to the surface, the measurements are more difficult and uncertain due to the surface irregularity, resulting in uncertainties higher than 11% (Gallet et al., 2011; Champollion et al., 2013; Gallet et al., 2014; Libois et al., 2014). Finally, an intercomparison exercise has recently shown that snow densities measured by different methods in the Swiss Alps agree within 9% and the vertical density variations are not completely captured (Proksch et al., 2016).

The objective of this study is to develop and validate a new method to determine the snow density near the surface from pas-

30 sive microwave satellite observations. The study is performed at Dome C (75°06′ S, 123°21′ E), in the East Antarctic Plateau where the French-Italian base of Concordia is located, combining in situ data of snow properties and electromagnetic modelling. Except for melting regions, the method has the potential for a global spatial coverage of Antarctic ice sheet which will be addressed in further work. Following Brucker et al. (2011), we first simulate the snow microwave emission and thus quantify its sensitivity to snow properties. Qualitatively, it is well known that the permittivity of snow is highly dependent on density (Mät-

zler et al., 1984; Warren and Brandt, 2008) and thus changes in the different layers of the snowpack. The electromagnetic reflections at each interface between layers with different densities (air–snow or internal snow–snow interfaces) are calculated with Fresnel equations, that use the snow permittivity and depend on the polarisation (Born and Wolf, 1999). As a consequence, snow density greatly influences the polarisation of microwave radiation, which was noted in previous studies (Shuman et al.,

5   1993; Shuman and Alley, 1993; Abdalati and Steffen, 1998; Liang et al., 2009; Champollion et al., 2013; Brucker et al., 2014; Leduc-Leballeur et al., 2015, 2017). Using the Dense Medium Radiative Transfer theory – Multi Layered (DMRT-ML, Tsang et al., 2000a; Roy et al., 2012; Picard et al., 2013; Dupont et al., 2013), we quantitatively determine the influence of surface snow density on microwave polarisation ratio. This relationship is then used to retrieve the density from satellite observations which are measured by the Advanced Microwave Scanning Radiometer – Earth observing system (AMSR-E) instrument. In

10   situ measurements of snow properties are used as input for the DMRT-ML model. Active microwave observations and in situ measurements of surface snow density are used to validate the method.

    Section 2 presents remote sensing and in situ data, and the microwave emission model. Section 3 presents some elements of the theoretical background on microwave radiative transfer and Section 4 the method to retrieve the surface snow density. Section 5 presents the time series of the retrieved surface snow density, and its validation and analysis.

2 Data & model

Satellite remote sensing datasets, measurements of snow properties and the microwave radiative transfer model are described in the three following sections.

2.1 Satellite observations

2.1.1 Passive microwave data

Passive microwave satellite observations were acquired at 18.7 and 36.5 GHz by AMSR-E instrument onboard Aqua satellite in dual-polarisation mode with an observation zenith angle of 54.8° during all the instrument lifetime, i.e. from 18 June 2002 to 4 October 2011. Daily-averaged brightness temperatures (T_B) at Dome C are extracted from the *AMSR-E/Aqua daily L3 25 km brightness temperature, sea ice concentration, and snow depth polar grids dataset* provided by the National Snow and Ice Data Center (NSIDC, Cavalieri et al., 2014). The pixel size is 25 km × 25 km and the total sensor error is around 0.6 K, according to the AMSR-E web-page (http://nsidc.org/data/docs/daac/amsre instrument.gd.html). The dataset contains, for every day, the mean of the daily-averaged ascending orbits and daily-averaged descending orbits. This typically represents seven overpasses per day at Dome C.

A detailed analysis of the spatial and temporal variability of passive microwave data close to Dome C is given by Long and Drinkwater (2000); Macelloni et al. (2007); Picard et al. (2009); Brucker et al. (2011). As in these previous studies, we assume that (1) one or few in situ measurements are sufficient to model the brightness temperature of an entire satellite pixel and (2) the pixel containing in situ measurements is representative of the satellite pixels around Dome C. These assumptions have been validated using ground-based radiometers by Picard et al. (2014), which found that the Dome C area was sufficiently homogeneous.

2.1.2 Active microwave data

Two complementary datasets of active microwave observations are used for comparison with the retrieved snow density. The first dataset was acquired by the Radar Altimeter 2 (RA-2) instrument onboard ENVIronment SATellite (ENVISAT) at 13.6 GHz (Ku-band) in full-polarisation mode with nadir looking. The dataset contains the total backscatter power from 12 March 2002 to 8 April 2012 along-track (Rémy et al., 2014). Radar backscatter corresponds to the ratio between the energy emitted by the satellite and the energy reflected by the snow surface, and is expressed in dB. Due to the 35 days of ENVISAT revisit time and the selection of 4 orbit tracks which are less than 17 km away from Concordia station, temporal sampling of RA-2 observations is typically 8–10 days. The spatial resolution over the Antarctic ice sheet along the tracks is 330 m, and the sensor precision to determine surface elevation is 0.047 m.

The second dataset of active microwave observations was acquired by the SeaWinds instrument onboard Quick SCATterometer (QuikSCAT) at 13.4 GHz in dual-polarisation mode. Zenith viewing angles are 46° and 54.1° for horizontal and vertical polarisations respectively. Normalised radar cross-sections σ^0 were extracted at Dome C from the *"egg" images of SeaWinds*

on QuikSCAT Enhanced Spatial Resolution Image Sigma-0 Products – Version 2 provided by the National Aeronautics and Space Administration – Scatterometer Climate Record Pathfinder (SCP web-page, Long and Daum, 1998; Early and Long, 2001; Long et al., 2001). The pixel size is $2.225\,\mathrm{km} \times 2.225\,\mathrm{km}$ and the relative error is 0.2 dB (Spencer et al., 2000; Early and Long, 2001). The dataset contains the daily-averaged backscatter coefficient by combining multiple passes of QuikSCAT
5 (near-polar orbit) from 19 July 1999 to 23 November 2009.

2.2 In situ snow measurements

Snow observations include the snow density near the surface and the vertical profiles (Fig. 1) of snow temperature, density and specific surface area (SSA).

2.2.1 Surface snow density

10 Three time series of snow density were measured at Dome C. The first set of measurements is from the CALVA program (CALibration-VAlidation of climate models and satellite retrieval, Antarctica coast to Dome C). Surface snow density was measured from 3 February 2010 to 4 October 2011 by using a cylinder cutter inserted horizontally (10 cm height and diameter of 5 cm) every 3 to 5 days. The value used here is the average of 3 measurements. The two other sets of measurements are from the project MAPME (Monitoring of Antarctic Plateau by means of Multi-Frequency Microwave Emission) funded by
15 PNRA (Programma Nazionale di Ricerche in Antartide). Second dataset contains surface the snow density measured from 18 December 2007 to 4 October 2011 by using a cylinder cutter of 25 cm height and a diameter of 4.5 cm. Measurements were performed at 0.1 m depth every 15 days in a snow stake network composed by 8 poles placed at 10 meter distance. The value used here is the average of 8 measurements. Last dataset contains the snow density measured in snowpits which were excavated every month. Density values were collected every 10 cm in the 0–1 m deep range. A single measurement was collected at each
20 depth of the snowpit.

The mean density value is $329\,\mathrm{kg\,m^{-3}}$, $344\,\mathrm{kg\,m^{-3}}$ and $321\mathrm{,kg\,m^{-3}}$ respectively for the CALVA dataset and the two PNRA dataset. The standard deviation is respectively $43\,\mathrm{kg\,m^{-3}}$, $40\,\mathrm{kg\,m^{-3}}$ and $54\,\mathrm{kg\,m^{-3}}$. Uncertainties associated to the three dataset are equal or higher (due to the low cohesion of surface snow) than the uncertainty estimated for classic density measurements (11%, Conger and McClung, 2009).

25 The spatial variability of surface snow density measurements has been assessed with 3 series of 40 measurements (measurements taken in every 1, 10 and 100 m). The averages and standard deviations are respectively $298.7 \pm 29.3\,\mathrm{kg\,m^{-3}}$, $317.6 \pm 24.7\,\mathrm{kg\,m^{-3}}$ and $307.9 \pm 59.8\,\mathrm{kg\,m^{-3}}$ for metre, decametre and hectometre scales. Considering all measurements (n=120), we found a mean density and standard deviation of $308.3 \pm 41.6\,\mathrm{kg\,m^{-3}}$. Under the assumption of a normal distribution of snow density measurements, the value $83.2\,\mathrm{kg\,m^{-3}}$ covers 95% of the distribution variance. This value represents
30 26.9% of the mean density and is assumed to represent the spatial variability of surface snow density measurements.
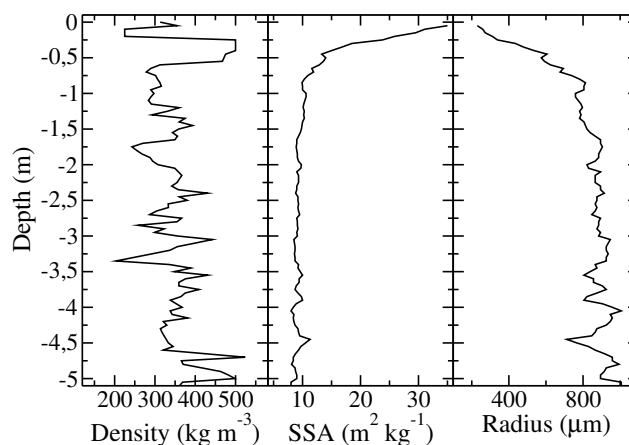
Figure 1. The profiles of snow density, SSA and DMRT-ML radius at Dome C, Antarctica. DMRT-ML radius is derived from SSA measurements and is the input of the model (Sec. 2.2.4 and Eq. 1 and 2).

2.2.2 Snow temperature profile

Snow temperature was recorded every hour from 1 December 2006 to 4 October 2011 and from the surface to 21 m depth with 35 probes initially installed every 0.1 m down to 0.6 m depth, every 0.2 m down to 2 m, every 0.5 m down to 5 m and every 1 m down to 21 m. The probes are located around 1 km West of the Concordia station. All probes (100 ohm platinium

5 resistance sensors with an accuracy better than ± 0.1 K at 223 K) were inter-calibrated with a precision of ± 0.02 K. The probes are continuously burying with time due to snow accumulation which is estimated of around 0.1 m yr^{-1} (Frezzotti et al., 2005; Arthern et al., 2006; Eisen et al., 2008; Brucker et al., 2011; Verfaillie et al., 2012; Frezzotti et al., 2013). Initial probe depths are corrected as function of the date measurements. In addition, the temperature measurements closest to the surface are deeper and deeper with time. It results that no measurements is taken in the upper snowpack. To correct for this issue, we extrapolate

10 the profiles using an exponential function between the uppermost probe in the snowpack and the temperature at the surface. The latter is approximated by the 2 m air temperature. Air temperature was extracted from the global ERA-Interim reanalysis provided by the European Centre for Medium-range Weather Forecasts (ECMWF, Dee and al., 2011). Passive microwave observations are daily, also we calculate daily-averaged temperature by averaging two hourly profiles (14:00 and 00:00 local time).

15 ### 2.2.3 Snow density profile

The snow density profile is considered constant and composed of two different datasets. The first dataset was measured in January 2010 by determining the mass and volume of snow/firn core samples every 5 centimetres, collected up to 20 m depth. However, the cohesion of the first 0.3 m of the snow core was very low and impossible to sample correctly. Thus, a second dataset was measured in December 2010 to complete the snow density profile from the surface down to 0.3 m depth. This

second dataset is an average of 13 short density profiles (up to 0.5 m depth) measured in snowpit with a dedicated cutter for Antarctic snow (Gallet et al., 2011).

The snow core and snowpit density profiles below 0.3 m depth are close together. Indeed, the mean and standard deviation of both profiles (0–0.5 m deep) are about $340 \pm 8\,\mathrm{kg\ m^{-3}}$ for the snow core dataset and about $355 \pm 21\,\mathrm{kg\ m^{-3}}$ for the snowpit
5   dataset. In addition, the overlapping part (between 0.3 and 0.5 m depth) shows similar values. Uncertainties associated to both methods are similar: at least 10% for measurements on snow/firn core samples (Arthern et al., 2010) and at least 11% for snow cutter measurements in a snowpit (Conger and McClung, 2009).

2.2.4   Snow specific surface area profile

The snow SSA is the surface area of ice crystals divided by the mass of snow (Dominé et al., 2006; Arnaud et al., 2011). Its
10   profile up to 20 m depth was measured in January and December 2010 using the POSSSUM instrument (Arnaud et al., 2011) and the Alpine Snow Specific Surface Area Profiler (ASSSAP, Champollion, 2013; Libois et al., 2014), which is a lightweight version of POSSSUM adapted for shallow snowpacks (maximun 2 m deep). These two instruments are based on the relationship between snow reflectance in the near-infrared domain and snow SSA (Dominé et al., 2006; Matzl and Schneebeli, 2006). Using a laser at 1310 nm illuminating the face of a snow hole and a specific data processing algorithm (Arnaud et al.,
15   2011), POSSSUM and ASSSAP instruments allow to measure the snow SSA as a function of depth in the field. Uncertainty associated to SSA measurements from POSSSUM is about 10% (Arnaud et al., 2011). Both instruments are very similar and have been compared multiple times, thereby ASSSAP uncertainty is considered to be 10% as well.

Larger errors were found above 0.3 m depth using POSSSUM device than using ASSSAP. Thus, we decided to use SSA measurements from ASSSAP for the first 0.3 m and POSSSUM observations below. SSA profiles from both instruments over-
20   lap between 0.3 m and 0.5 m depth and show very close values. Averaged SSA values from ASSSAP is $13.2\,\mathrm{m^2\ kg^{-1}}$ and $13.9\,\mathrm{m^2\ kg^{-1}}$ for POSSSUM. Due to an artefact that increases the measured SSA when the hole is drilled for snow below 5 m (Picard et al., 2014), we removed the measured values and replaced them by a constant value (SSA_{5m}). This value is optimised following Brucker et al., 2011 (Sec. 5.1).

The snow SSA is not directly used in DMRT-ML model. The snow parameter that characterizes the snow grain size in the
25   electromagnetic model ($r_{DMRT-ML}$) is related to the optical radius (r_{opt}). The relationships between snow SSA, DMRT-ML radius and optical radius are given by the following equations:

$$r_{DMRT-ML} = \phi \cdot r_{opt} \tag{1}$$

$$SSA = (3 \cdot \phi)/(\rho_{ice} \cdot r_{opt}) \tag{2}$$

where ϕ is a snow microstructure parameter that depends on the shape of snow crystals, the stickiness and the size distribution
30   of ice crystals (Brucker et al., 2011; Roy et al., 2012; Dupont et al., 2013) and ρ_{ice} is the density of ice, i.e. $917\,\mathrm{kg\ m^{-3}}$. ϕ parameter is optimised (as in Brucker et al., 2011, Sec. 5.1).

2.3 Microwave emission model

2.3.1 Snow microwave emission

The snow microwave emission model DMRT-ML (Picard et al., 2013) has already been applied and validated in several studies (Brucker et al., 2011; Roy et al., 2012; Dupont et al., 2013; Picard et al., 2014) and is freely available at http:
5 //pp.ige-grenoble.fr/pageperso/picardgh/dmrtml/. It allows the computation of the top-of-snowpack emerging brightness temperature for a given snowpack at different viewing angles, at different frequencies and at both vertical and horizontal polarisations. Two parts compose the model: (1) the DMRT theory to calculate the absorption and scattering coefficients for all snow layers – in the model, the snowpack is composed of horizontally semi-infinite and vertically homogeneous snow layers of dense ice spheres, completely defined by the layer thickness, temperature, density and optical radius of snow – and (2) the
10 DIScrete Ordinate Radiative Transfer method (DISORT, Jin, 1994) to propagate the thermal emission of each snow layer from the bottom of the snowpack to the atmosphere. DISORT accounts for multiple scattering between layers. Layers are assumed planes, parallels and much thicker than the wavelength.

We use the model in a non-sticky grain configuration, i.e. grains which do not form aggregates, and with a unique optical radius of snow grains, i.e. no grain size distribution. Snow crystal aggregates are not considered in this study because ϕ
15 parameter used to convert snow SSA into optical radius partly integrates this snow property (Roy et al., 2012; Lowe and Picard, 2015). We also use a semi-infinite bottom snow layer to consider the firn of the Antarctic ice sheet. In addition, two criteria must be respected in the framework of DMRT theory: snow density less than 300–350 kg m^{-3} (Liang et al., 2006; Tsang et al., 2008) and low optical radius with respect to the wavelength (Rayleigh scattering). The latter is always respected in our study since $r_{DMRT-ML}$ never exceed 0.6 wavelengths and most of the time is lower than 0.1. Regarding the density
20 sometimes higher than 350 kg m^{-3} in our profile (Fig. 1), Picard et al. (2013) explained that the deviation in scattering and absorption coefficients remains moderate.

2.3.2 Atmospheric contribution

The atmosphere attenuates the microwaves emission emerging from the surface and itself emits microwaves due to its own temperature (Rosenkranz, 1992). Although this effect is low over Antarctica Plateau, because of the low atmospheric humidity
25 and the small size of scatterers in the atmosphere (Walden et al., 2003; Genthon et al., 2010), both effects are taken into account in our modelling on a daily basis with a simple non-scattering radiative transfer scheme. Top-of-atmosphere (TOA) brightness temperatures are computed using the method and equations from Rosenkranz (1992) and following Picard et al. (2009). Upward and downward atmospheric T$_B$s are calculated using atmospheric temperature and moisture profiles from ERA-Interim reanalysis. The transmission coefficient is 0.960 at 37 GHz and 0.987 at 19 GHz, and the downward cosmic TOA
30 T$_B$ is 2.75 K.

3 Theoretical background in microwave remote sensing

Some elements of the theoretical background in microwave satellite remote sensing are described in the next two sections.

3.1 Passive microwave remote sensing

We use the brightness temperature polarisation ratio (PR) at 19 and 37 GHz to increase the sensitivity of passive microwave
observations to surface properties (Shuman et al., 1993; Surdyk, 2002a; Champollion et al., 2013):

$$PR_\nu = \frac{T_{\mathrm{B}}(\nu, h)}{T_{\mathrm{B}}(\nu, v)} \tag{3}$$

where $T_{\mathrm{B}}(\nu, \alpha)$ is the brightness temperature, ν the frequency and α the polarisation.

Champollion et al. (2013) showed that PR, at AMSR-E incidence angle which is close to the Brewster angle for the air–
snow interface, mainly depends on the snow density near the surface, the surface roughness and the vertical snow stratification,
i.e. abrupt changes in the snow density profile. We consider flat interfaces which neglect the roughness influence on PR (the
relevance of this assumption is explained in Sec. 5.5). Consequently, polarisation ratio is a non-linear combination of surface
and internal reflections (Leduc-Leballeur et al., 2017).

In order to understand the polarisation ratio evolution, two cases are explored: (1) snow properties vary with depth but are
constant in time and (2) snow properties also vary with depth. For case (1), the PR evolution is only due to changes in the
snow density near the surface. For case (2), PR evolution is also influenced by changes in the snow density stratification. Snow
evolution is mainly influenced by atmospheric conditions. The surface is first affected and then atmospheric influence diffuses
deeper into the snowpack. This process is slow on the Antarctica Plateau (Surdyk, 2002b; Brucker et al., 2011; Picard et al.,
2014; Libois et al., 2014) and implies a slower evolution of snow deeper into the snowpack than near the surface. As a result,
the PR evolution is primarily influenced by surface snow density variations (the relevance of this assumption is explained in
Sec. 5.5).

3.2 Active microwave remote sensing

The signal returned by the snowpack is a complex combination of surface and volume scattering (Rémy and Parouty, 2009;
Rémy et al., 2014; Tedesco, 2015; Adodo et al., 2018). The surface to subsurface signal ratio is used to determine the main
contributor to radar backscatter observations. On the East Antarctica Plateau, this ratio is high (Lacroix et al., 2008, 2009)
and thus, surface echo is the main contributor to the radar backscatter at Dome C. Consequently, the long-term evolution of
ENVISAT observations mainly depends on surface snow density and roughness.

Because the incidence angles of SeaWinds instrument are close to the Brewster angle for the air–snow interface, the surface
reflection at vertical polarisation is weakly influenced by the near surface snow density. Consequently, the evolution of the
radar backscatter coefficient at vertical polarisation is mostly dependent on surface roughness changes. Therefore, considering
the independence of volume scattering to the polarisation (Tsang et al., 2000b; Picard et al., 2013) as well as the independence

of surface roughness effect to the polarisation (Ulaby et al., 1982; Adodo et al., 2018), we defined the radar polarisation ratio (RPR) to be primary influenced by the snow density near the surface (Liang et al., 2008):

$$RPR = \frac{\sigma_h^0}{\sigma_v^0} \simeq \frac{r_{h,surface}^0}{r_{v,surface}^0} \tag{4}$$

where σ^0 is the radar backscatter coefficient, r^0 is the part of backscatter coefficient considering only the surface reflection, h
and v are the polarisations. For simplicity, ν index is not written.

4 Method

The different steps of the method to retrieve the surface snow density are described in this section. Surface density variations are deduced from the PR evolution. However, to correctly simulate PR evolution, we first need to simulate PRs mean state.

A. In a first step, we follow the forward modelling approach of Brucker et al., 2011 to simulate the time series of brightness temperatures using the vertical profiles of snow properties which are kept constant with time except for the temperature. From the simulated brightness temperatures, we calculate the time series of polarisation ratios, and show the correct simulation of the mean polarisation ratios and the poor modelling of their temporal variations.

B. In a second step, we theoretically simulate the polarisation ratio variations to properties of a 0.03 m snow layer on top of the snowpack (as in Leduc-Leballeur et al., 2015, 2017), and show the strong relationship between PR at 37 GHz and the density of this surface layer.

C. The third step corresponds to the retrieval algorithm itself. We estimate the time series of surface snow density by minimising the deviations between modelled and observed polarisation ratio at 37 GHz.

Some studies have reported the high vertical snow stratification around Dome C (Gallet et al., 2014; Picard et al., 2014). They observed very dense and thick snow layers (about $500 \, \mathrm{kg \, m^{-3}}$ for 0.3–0.5 m thick), and thin and low-density layers (less than $150 \, \mathrm{kg \, m^{-3}}$ for a thickness of few centimetres). The poor modelling of the horizontally polarised brightness temperature could be due to an underestimation of the snow stratification (Macelloni et al., 2007; Brucker et al., 2011; Champollion et al., 2013; Picard et al., 2013; Leduc-Leballeur et al., 2015). In order to correctly simulate the mean horizontally polarised brightness temperatures and thus the mean polarisation ratios, we added, at 0.1 m and 0.2 m depth in our snow density profile, two layers of 0.1 and 0.2 m thick with a density equal respectively to 225 and $500 \, \mathrm{kg \, m^{-3}}$.

5 Results & discussion

The results of the different steps to retrieve the surface snow density are presented in the three next sections. The fourth section is dedicated to the comparison and validation of the retrieved density, and the last section examines the different sources of uncertainties.

5 ### 5.1 Time series simulation

TOA horizontally– and vertically–polarised brightness temperatures at 19 and 37 GHz – written $T_{\mathrm{B}}(19,\mathrm{V})$, $T_{\mathrm{B}}(19,\mathrm{H})$, $T_{\mathrm{B}}(37,\mathrm{V})$ and $T_{\mathrm{B}}(37,\mathrm{H})$ – are simulated with the DMRT-ML model during the 3 years (from 1 December 2006 to 31 December 2009) when the temperature profiles were recorded. The two parameters SSA_{5m} and ϕ are optimised during this period of calibration, by minimising the Root Mean Square Error (RMSE) between the modelled and observed $T_{\mathrm{B}}(19,\mathrm{V})$ and $T_{\mathrm{B}}(37,\mathrm{V})$. As

10 in Brucker et al. (2011), only the vertical polarisation is used because of its high sensitivity to snow SSA and reduced sensitivity to density changes. TOA brightness temperatures are then simulated during nearly 2 years of validation (from 1 January 2010 to 4 October 2011) using the optimised SSA_{5m} and ϕ parameters. RMSEs are defined by the following equations:

$$RMSE_{\nu,\alpha} = \sqrt{\frac{1}{n} \cdot \sum_{i=1}^{n} \left(T_{\mathrm{B},i}^{obs}(\nu,\alpha) - T_{\mathrm{B},i}^{mod}(\nu,\alpha) \right)^2} \tag{5}$$

$$RMSE_{\nu} = \sqrt{0.5(RMSE_{\nu,v}^2 + RMSE_{\nu,h}^2)} \tag{6}$$

15 $$RMSE = \sqrt{\frac{1}{p} \cdot \sum_{\nu,\alpha} RMSE_{\nu,\alpha}^2} \tag{7}$$

with n the number of observations, $T_{\mathrm{B},i}^{obs}(\nu,\alpha)$ and $T_{\mathrm{B},i}^{mod}(\nu,\alpha)$ the observed and modelled brightness temperatures at ν frequency α polarisation, and $p = 4$ the number of polarisations and frequencies used.

The time series of observed and modelled brightness temperatures are shown in the Figure 2. The optimised SSA_{5m} and ϕ parameters are respectively equal to $10.1\,\mathrm{m^2\,kg^{-1}}$ and to 2.5, in the range to those found by Brucker et al. (2011) and Picard

20 et al. (2014) respectively 2.8 and 2.3, with a RMSE of 1.6 K. Observed brightness temperatures are well reproduced by DMRT-ML model both in term of absolute value and evolution, except for 19 GHz at horizontal polarisation. The RMSE calculated by excluding $T_{\mathrm{B}}(19,\mathrm{H})$ is indeed 2.6 K whereas RMSE $_{19,h}$ is 7.4 K. Table 1 summarises all errors between observed and modelled T_{B}s. The RMSE during the calibration and validation periods are very close showing the high performance of the optimisation. We also found a slightly improvement of the modelled $T_{\mathrm{B}}(19,\mathrm{H})$ compared to Brucker et al. (2011) with an

25 RMSE $_{19,h}$ of 7.4K instead of 8–10 K. These results confirm the representativeness of the in situ measurements for the satellite pixel encompassing Dome C (25 km × 25 km).
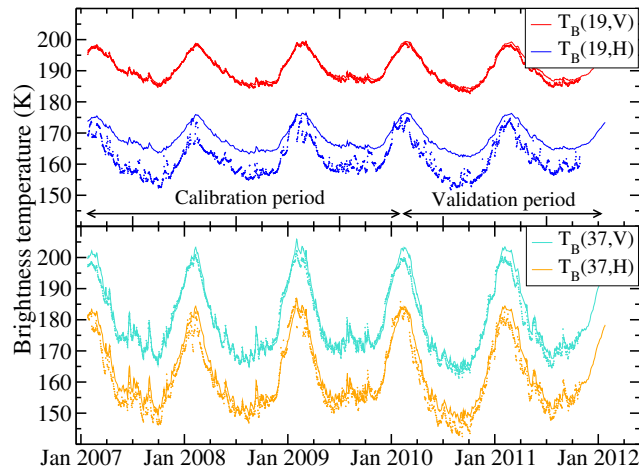
Figure 2. Time series of modelled (lines) and observed (dots) brightness temperatures, at 19 and 37 GHz and at vertical and horizontal polarisations ($T_\mathrm{B}(19,\mathrm{V})$, $T_\mathrm{B}(19,\mathrm{H})$, $T_\mathrm{B}(37,\mathrm{V})$, $T_\mathrm{B}(37,\mathrm{H})$) at Dome C, Antarctica, during the calibration period (2007–2009) and the validation period (2010–2011).

	$RMSE_{19,v}$	$RMSE_{19,h}$	$RMSE_{37,v}$	$RMSE_{37,h}$
Calibration period	0.63	7.6	2.1	3.7
Validation period	1.6	7.2	3.6	4.1

	$RMSE_v$	$RMSE_h$	$RMSE$
Calibration period	1.6	6.0	4.4
Validation period	2.8	5.9	4.6

Table 1. Errors between modelled and observed brightness temperatures (K) for the calibration and validation periods.

The polarisation ratio evolution, calculated from the simulated brightness temperatures, does not reproduce the observed variations, and the 5 year average of modelled PR_{19} overestimates by 0.033 the observations (Fig. 3). This represents around 46% of the maximum amplitude of observed PR_{19} variations. On the other hand, mean PR_{37} is well modelled. The simulated mean PR_{37} is indeed 0.904 whereas observed mean PR_{37} is 0.896. The difference represents only 11% of the maximum

5   amplitude of observed PR_{37} variations. Table 2 summarises all errors between observed and modelled PRs.

The poor simulation of the mean PR_{19} comes from an incorrect simulation of $T_\mathrm{B}(19,\mathrm{H})$ which, as explained in Arthern et al. (2006) is mainly due to the stratification of the snowpack. Because PR_{37} is well reproduced, and considering that penetration depth is respectively around 5 m and 1 m for 19 and 37 GHz (Surdyk, 2002b), the stratification in the top first meter of the snowpack is adequately represented. Hence, the discrepancy between observed and modelled PR_{19} is probably because of a

10   too weak stratification below 1 m depth, and further works can address this issue by increasing the stratification deeper into the snowpack. The poor simulation of the mean PR_{19} is not a major issue in this work since we study the time variations of
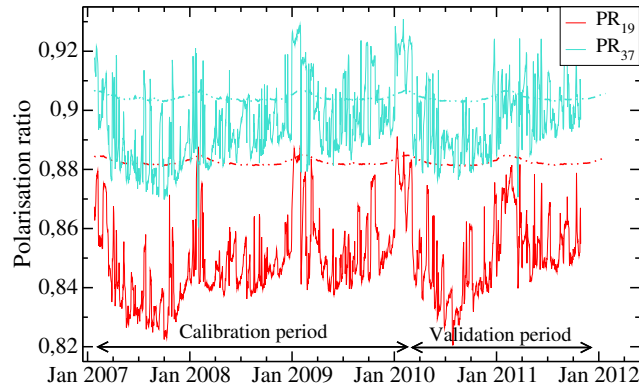
Figure 3. Time series of modelled (lines) and observed (dots) polarisation ratios at 19 and 37 GHz (PR_{19} and PR_{37}) at Dome C, Antarctica, during the calibration period (2007–2009) and the validation period (2010–2011).

	$RMSE_{PR,19}$	$RMSE_{PR,37}$	$RMSE$
Calibration period	0.039	0.017	0.030
Validation period	0.031	0.011	0.023

Table 2. Errors between modelled and observed polarisation ratios for the calibration and validation periods.

polarisation ratios. However, we decided to exclude 19 GHz data frequency in the following of this study in order to avoid introducing bias in the retrieved density.

In contrast to the long-term average, the seasonal and faster variations of the polarisation ratio at 37 GHz are not reproduced. We explain this by the fact that the evolution of polarisation ratio is mainly governed by variations of the snow density close to the surface whereas we have considered here the snow density profile constant with time in our simulation.

5.2 Sensitivity analyses

In order to represent the snow evolution close to the surface and thus to simulate PR_{37} variations, a thin layer (0.03 m thick) is added on the top of the previous snowpack. Then, a sensitivity analysis of PR_{37} to the snow parameters of this top layer is performed. The PR_{37} variations due to changes of a single snow parameter of the upper layer (density, temperature, SSA or thickness) and keeping constant the other variables (equal to those of the next layer) are shown in Figure 4. The simulations are performed for two temperature profiles corresponding to typical summer and winter conditions (January 1$^{\text{st}}$ and August 1$^{\text{st}}$).

The results clearly show that only the density of the first layer can significantly change the polarisation ratio. For comparison, large variations of SSA from 10 to 100 m^2 kg^{-1}, thickness from 0.01 m to 0.1 m and temperature from 190 K to 270 K, result respectively in small changes of PR_{37} of around 2%, 5% and 1.5% of the PR variations caused by density changes from 150 to 450 kg m^{-3}. In addition, variations of snow density between 150 to 450 kg m^{-3} permit to simulate the observed range of temporal PR variations between 0.88 and 0.92. Moreover, this simulation shows the weak influence of the temperature profile
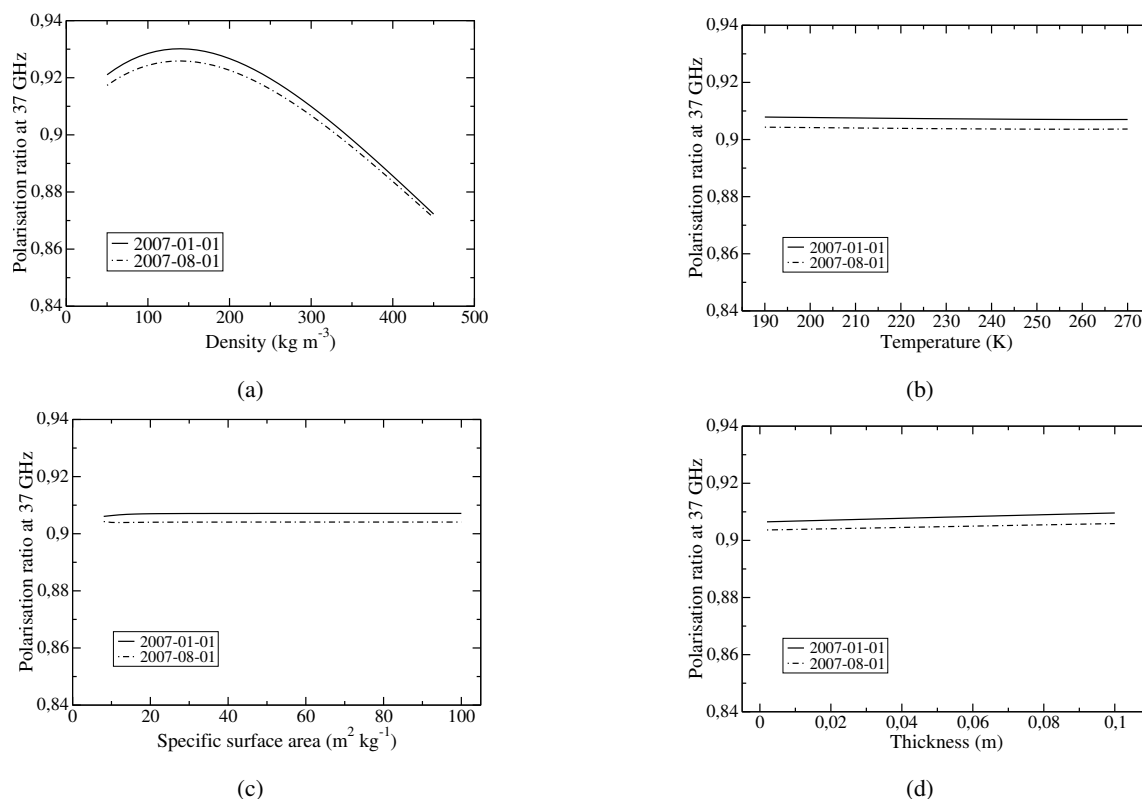
Figure 4. PR_{37} variations caused by changes in snow properties of the top layer: (a) density, (b) temperature, (c) SSA and (d) thickness. The two different dates correspond to typical winter and summer temperature profiles.

on polarisation ratio. The larger variation due to the different temperature profiles is 0.0043 which represents only 7.25% of the larger PR variation caused by surface density changes (from 150 to $450 \, \mathrm{kg \, m^{-3}}$). This sensitivity analysis demonstrates the strong relationship between the polarisation ratio at 37 GHz and surface snow density, and herewith show the possibility to retrieve the density ρ_{sat} from the PR_{37} satellite observations.

5   **5.3   Surface snow density evolution**

Surface snow density ρ_{sat} is estimated every day by minimising the RMSE between the observed and modelled PR_{37} by changing only the snow density of the top layer. The RMSE minimisation is done by a Newton approach (scipy.optimize.newton function of python language). This method ensures a quick convergence (typically after 3–5 iterations) with a residual RMSE less than 0.001. That translates into a precision of surface snow density equal to $3.5 \, \mathrm{kg \, m^{-3}}$. We use a constant vertical
10   profile of temperature and equal to the 5-year average of the vertical temperature profile measured in the field. This choice is motivated by the fact that no temperature data are available before December 2006. However, the results are weakly affected by this assumption (Sec. 5.5). Because of the 5-year average, the temperature profile is also nearly constant with depth around
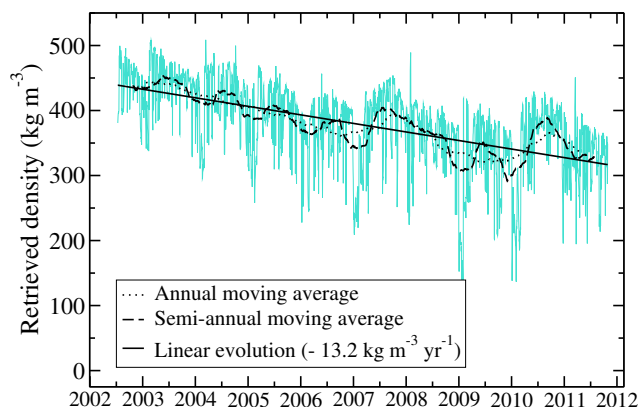
Figure 5. Time series of the snow density near the surface ρ_{sat} at Dome C, Antarctica, retrieved from AMSR-E passive microwave observations and covering the period from 18 June 2002 to 4 October 2011.

218.5 K, which is the mean annual temperature at Dome C between 2006 and 2011 (periods where temperature measurements are available). SSA and thickness of the top snow layer are $60.0\,\mathrm{m^2\,kg^{-1}}$ and 30 mm respectively (Champollion, 2013; Libois et al., 2015; Leduc-Leballeur et al., 2017). The retrieved density is representative of the mass of snow integrated over 3 times the wavelength, which around corresponds to the top 3 centimetres of the snowpack (Ulaby et al., 1981, 1982; Tsang et al.,

5   2000b), the wavelengths of AMSR-E being 8.2 mm at 37 GHz in the air. This representativeness can slightly change (between 2 cm and 5 cm) depending on the type of crystals present on the surface (Leduc-Leballeur et al., 2017).

The time series of ρ_{sat} from 18 June 2002 to 4 October 2011 shows fast and large variations, an annual cycle and a pluri-annual decrease trend (Fig. 5). The fast variations have a maximum amplitude of about $200\,\mathrm{kg\,m^{-3}}$ for a typical time scale of few days and are certainly linked to wind and precipitation, that are frequent atmospheric processes with potentially a

10   large impact on snow density (Picard et al., 2012; Champollion et al., 2013; Libois et al., 2014; Brucker et al., 2014; Leduc-Leballeur et al., 2017). Hoar formation on the surface, for a typical duration of one week, can also greatly impact surface snow density (Champollion et al., 2013).

The annual cycles have a mean amplitude of about $30\,\mathrm{kg\,m^{-3}}$ with two extreme years (2007 and 2010 when the amplitude reached nearly $60\,\mathrm{kg\,m^{-3}}$) which correspond to two summers with low cumulated snowfall and a large increase of the snow

15   Grain–Index (Picard et al., 2012). These conditions probably involve intense metamorphism of the snow near the surface during the summer, and can potentially result in longer presence of hoar crystals on the surface or larger hoar crystals (Champollion et al., 2013), that decrease surface snow density (Gallet et al., 2014). Years 2008 and 2011 are also particular with the absence of annual cycle.

A pluri-annual decrease trend of $-13.2\,\mathrm{kg\,m^{-3}\,yr^{-1}}$ is observed over the 10 years of AMSR-E observations. This evolution

20   represents a significant change and could result from an increase of precipitation (recent snow being usually less dense than old snow), a decrease of wind speed (wind usually compact surface snow) or a longer and more often presence of hoar/sublimation

crystals on the snow surface (hoar/sublimation crystals being usually less dense than small rounded grains, Dominé et al., 2006).

5.4 Comparison and validation

5.4.1 Comparison with in situ measurements

Figure 6 shows the time series of ρ_{sat} and the three time series of the in situ surface snow density. We obtain a remarkable agreement even if different daily and weekly variations are observed. The range of observed density is 150-425 kg m^{-3} for in situ measurements as for satellite estimation during the overlap period. From February 2010 to October 2011 (when all datasets are available), the mean surface snow density is 339.8 ± 58.8 kg m^{-3}, 304.2 ± 48.7 kg m^{-3}, 346.4 ± 43.9 kg m^{-3} and 303.4 ± 57.6 kg m^{-3} respectively for the satellite, CALVA measurements, PNRA-stake and PNRA-pit measurements. The datasets are consistent together and the mean values are within the uncertainty range. We observe however 3 notable differences: 1) measurements in snowpits are regularly lower by 35–40 kg m^{-3} than satellite and stake estimates ; 2) spatial variability of snow density (41.6 kg m^{-3}) is of the same order of magnitude as the differences between the mean value of datasets (higher difference is 43 kg m^{-3}) ; 3) satellite density (standard deviation is 63.5 kg m^{-3}) is generally more variable than the in situ measurements (standard deviations are 43, 40 and 54 kg m^{-3}). The last observation (3) could be the result of the different thickness for the retrieved satellite surface snow density (2–5 cm) compared with the in situ measurements (about 5 cm for CALVA measurements and 10 cm for PNRA measurements).

The four time series of surface snow density show a pluri-annual decreasing trend. The linear trends during the common period (February 2010 to October 2011) for the 4 time series are in the same order of magnitude, between -20 and -40 kg m^{-3} yr^{-1}. The trend over 10 years of the satellite retrieved density is -13 kg m^{-3} yr^{-1} and the trend over 4 years of the two PNRA in situ datasets are -6 kg m^{-3} yr^{-1} and -8 kg m^{-3} yr^{-1}.

5.4.2 Comparison with existing studies

Gallet et al. (2014) measured the snow density very close to the surface and found a range of density between 125 and 165 kg m^{-3} for the first centimetre of snow and between 202 and 290 kg m^{-3} for the second centimetre. In Gallet et al. (2011), the authors sampled the density near the surface in snowpits (at around 2 cm depth) and found a snow density range from 146 to 325 kg m^{-3}. Libois et al. (2014) measured the snow density near the surface between 150 and 360 kg m^{-3}. In a study dedicated to spatial variability, Picard et al. (2014) found a range of snow density from 270 to 520 kg m^{-3} in the first metre of the snowpack. During the 2010–2011 summer campaign at Dome C, we measured surface snow densities between 270 and 380 kg m^{-3}. We also measured the density of hoar crystals present at the surface. The mean value was 178 kg m^{-3} in agreement with the measurements of hoar crystals density performed in Greenland of 150 kg m^{-3} (Shuman et al., 1993). All surface snow density measurements are coherent together showing lower density values when surface snow is covered by hoar crystals (about 125–178 kg m^{-3}). The surface snow densities retrieved from satellite are between 136 and 508 kg m^{-3}. The average density over the 10 years is 377 kg m^{-3} and the standard deviation is 63.5 kg m^{-3}. The retrieved densities are

(a) The whole period.

(b) Focus on the last 2 years.

(c) Focus on the trends.
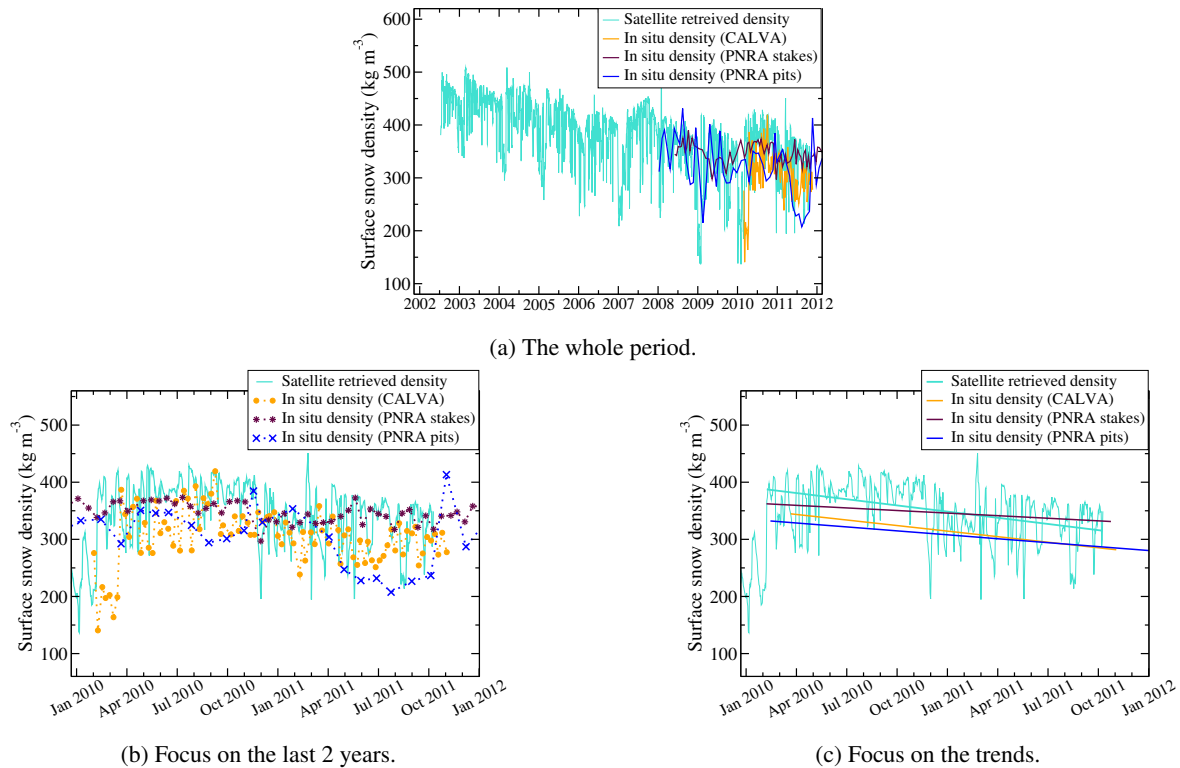
Figure 6. Time series of the snow density near the surface at Dome C, Antarctica, retrieved from AMSR-E passive microwave observations and measured in the field (3 different datasets) from 18 June 2002 to 4 October 2011 (a). The graph (b) focuses on the last two years and the graph (c) on the trends during the last two years.

slightly higher than those found in existing studies or those measured during the 2010–2011 summer campaign (upper bound is $380 \, \mathrm{kg \, m^{-3}}$). The average of ρ_sat is close to the mean density of the 3–5 first metres of snow at Dome C, which is about 350–$360 \, \mathrm{kg \, m^{-3}}$ with a range between 250–260 and 480–$490 \, \mathrm{kg \, m^{-3}}$ (Frezzotti et al., 2005; Brucker et al., 2011; Verfaillie et al., 2012; Zwaaftink et al., 2013). The time series of ρ_sat shows a large range of density and all its values have frequently
5 been observed in previous field studies.

Champollion et al. (2013) linked the presence of hoar crystals on the snow surface and passive microwave observations. We reassess here this former study by examining the variations of the retrieved density during hoar formation and disappearance events from 23 November 2009 to 4 October 2011. Among the 14 hoar formation events observed with an automatic camera in the field, ρ_sat decreases for 10 of them, with an average amplitude of $-49.0 \, \mathrm{kg \, m^{-3}}$ in a single day ; For the 4
10 remaining events, ρ_sat slightly increases by $15.0 \, \mathrm{kg \, m^{-3}}$. For the 15 hoar disappearance events observed from the ground, ρ_sat increases as expected for 14 of them, with an average amplitude of $+47.0 \, \mathrm{kg \, m^{-3}}$; for the remaining event, ρ_sat decreases by $-10.0 \, \mathrm{kg \, m^{-3}}$. The good agreement between the quick ρ_sat variations and hoar evolution confirms the precision of the detec-

tion of density changes from AMSR-E. The influence of surface properties on passive microwave observations has also been confirmed in Brucker et al., 2014; Leduc-Leballeur et al., 2017.

5.4.3 Comparison with active microwave observations

QuikSCAT 7-year time series of the residual backscatter at vertical and horizontal polarisation and the radar polarisation ratio
5 are shown in Figure 7. The time series are smoothed with a 5 day moving window in order to reduce the influence of the QuickSCAT viewing angle variations. The 3 curves feature quick variations (daily to monthly), an annual cycle (clearly visible only after 2004 for RPR time series) and a pluri-annual trend. The linear trend of vertical polarised backscatter is nearly constant whereas the time series of horizontal polarisation backscatter shows a linear decrease of -0.03 dB yr^{-1}. The RPR time series increases by 0.0042 yr^{-1} which is comparable to the observed trends of passive microwave observations: 0.0032 yr^{-1}
10 for PR_{37}, 0.0033 yr^{-1} for PR_{19} and 0.0024 yr^{-1} for PR_{10}. We can conclude from the absence of trend in σ_v^0 time series that surface roughness has not evolved much between 2002 and 2009 at Dome C, Antarctica. Furthermore, the negative trend of the horizontal backscatter and the positive trend of RPR are certainly associated to a slow decrease of surface snow density since 2002, and thus QuickSCAT observations confirm the density retrieved from AMSR-E satellite.

ENVISAT/RA-2 time series of the residual backscatter at 13.6 GHz is presented in Fig. 8. The time series shows a super-
15 imposition of a negative linear trend of -0.1 dB yr^{-1}, an annual cycle with large amplitude (between 0.4 and 1.2 dB yr^{-1}) and weekly oscillations. These latter variations are residual biases between ascending and descending passes, and are removed by smoothing the time series. The annual cycles are caused by changes in volume echo of the ENVISAT observations (Adodo et al., 2018).

The pluri-annual trend of ENVISAT/RA-2 observations of -0.1 dB yr^{-1} comes mainly from a progressive evolution of sur-
20 face snow density or surface roughness (Sec. 3.2). Lacroix et al. (2008, 2009) quantified the influence of individual snow parameters to radar backscatter by modelling the waveform of the altimetric signal. We use here the relationship found by Lacroix et al. (2008, 2009) to convert backscatter coefficient changes to surface snow density variations: for a smooth surface, a surface snow density increase of 100 kg m^{-3} results in a backscatter coefficient increase of 0.3 dB at Ku-band. It results an estimation of the surface snow density decrease from ENVISAT/RA-2 observations by around -30 kg m^{-3} yr^{-1} which is about 2.3 times
25 larger in amplitude than the trend found from AMSR-E observations. The backscatter coefficient is reduced by an increase of the surface roughness, and thus the linear trend could also be affected by changes in surface roughness (Adodo et al., 2018).

5.5 Uncertainties and discussion

We first present an assessment of the uncertainties and then discuss the importance of several caveats that may affect the accuracy of ρ_{sat}: the effects of using a constant vertical profile of temperature, of variations of the azimuthal viewing angle,
30 and of considering the temporal evolution of the surface roughness and the snow deeper into the snowpack.
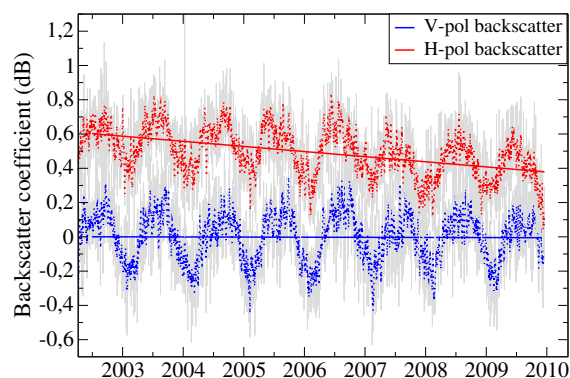
(a) Vertical and horizontal backscatter coefficient.
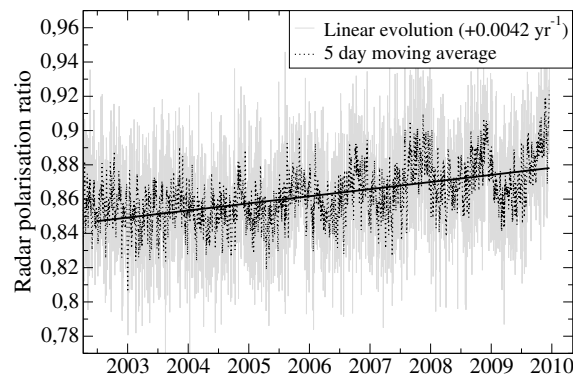
(b) Radar polarisation ratio.

Figure 7. Time series of the residual vertical and horizontal backscattering coefficients, and the radar polarisation ratio, from QuikSCAT at Dome C, Antarctica, from 18 June 2002 to 23 November 2009. Grey lines are the original data and red, blue and black dots are the 5 day moving averages. Note the different vertical axis scales for H-pol and V-pol.

5.5.1 Uncertainty assessment

We use here the signal-to-noise ratio (SNR) to characterize the significance of our results. SNR is the ratio between the mean of the observed data over the standard deviation of the background noise. In our time series of surface snow density, we assume that the standard deviation of quick variations as noise even though part of it may be a natural signal. That gives an

5   upper limit of the noise. We found a SNR of 5.9. This value is high enough to conclude that a real signal emerges from the noise and thus the negative trend of surface snow density is significant at Dome C. Furthermore, the spatial variability of surface snow density ($41.6 \, \mathrm{kg \, m^{-3}}$) was measured near Concordia Station which is smaller than the standard deviation of the retrieved density ($63.5 \, \mathrm{kg \, m^{-3}}$). That indicates that variations of the retrieved density are not only due to the spatial variability. However, the spatial variability is not directly taken into account in the retrieved density. That results in uncertainties in the

10   retrieved density (Brucker et al., 2011; Picard et al., 2014). In the last study, authors found an alternation every 15–25 m of dense/hard snow and light/loose snow areas. They found smaller density variations at larger scales which indicate that the
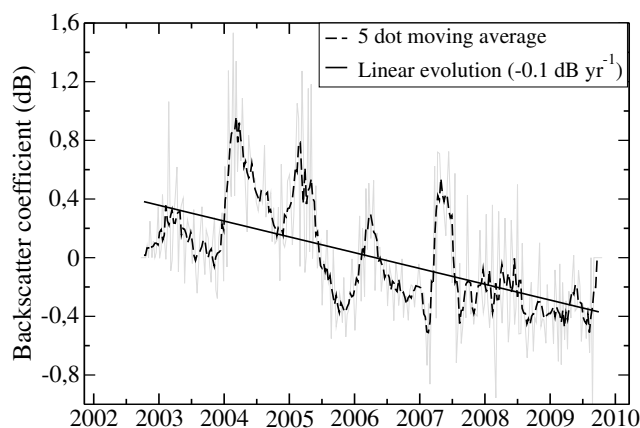
Figure 8. Time series of the backscattering coefficient from ENVISAT/RA-2 at Dome C, Antarctica, from 12 March 2002 to 8 April 2012.

spatial variability of density exists at smaller scale than AMSR-E satellite pixel ($625 \, \text{km}^2$). They conclude that changes in emissivity, as observed by Lacroix et al. (2009), might be solely due to changes in the proportion of dense/hard snow features without significant changes in surface properties on the two faces. In this study, we conclude that the decrease of surface snow density can not be solely due to a decrease in the proportion of dense/hard snow features because the trend is observed in other

5   datasets which have very different spatial scales from few metre scale for in situ measurements to hectometre/kilometre scale for active microwave observations.

5.5.2   Caveats affecting the accuracy of the retrieved density

The vertical profile of temperature

Figure 9 shows the time series of ρ_{sat}, using either the vertical temperature profile of the day or a temperature profile constant

10   with time as used in Section 5.3 to retrieve the surface snow density. Both curves overlap each other very well which confirms the small influence of the temperature profile on ρ_{sat}. This is not surprising since we already showed the limited influence of temperature changes of the upper layer (Fig. 4). When considering a constant profile of temperature, the standard deviation of the retrieved density is $59.5 \, \text{kg} \, \text{m}^{-3}$, slightly higher than when the actual temperature profile of each day is used ($57.4 \, \text{kg} \, \text{m}^{-3}$). The overall trend of the retrieved snow density is $-11.2 \, \text{kg} \, \text{m}^{-3} \, \text{yr}^{-1}$ and $-10.2 \, \text{kg} \, \text{m}^{-3} \, \text{yr}^{-1}$ respectively when using the

15   vertical temperature profile of each days or a constant profile of temperature.

The azimuthal viewing angle

If satellite observations were performed over an isotropic surface, the azimuth angle would be without effect on the measurements. This is not the case over the Antarctic Plateau as many studies demonstrated the effect of azimuthal variations on satellite measurements (?Shuman et al., 1993; Li et al., 2008; Narvekar et al., 2010). However, this effect is weak in our

20   study because we use daily-averaged observations and the first two components of the Stokes vector that minimise the effect
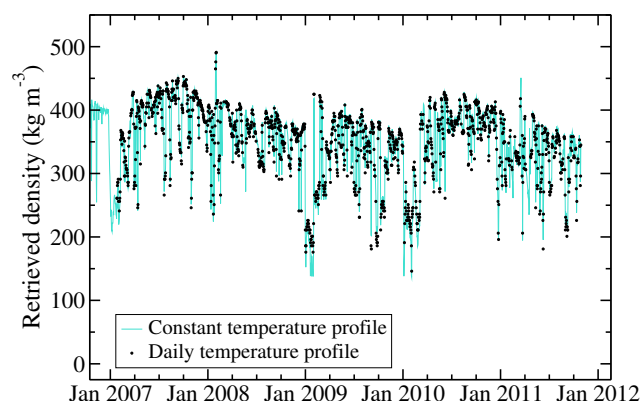
Figure 9. Time series of the snow density near the surface ρ_{sat} at Dome C, Antarctica, retrieved from AMSR-E passive microwave observations and covering the period from 1 December 2006 to 4 October 2011: (black dots) using the temperature profile of each day and (solid grey line) using a temperature profile constant in time.

of variations of the azimuthal viewing angle (Long et al., 2001; Li et al., 2008; Narvekar et al., 2010). Furthermore, passive microwave are less sensitive than active microwave to the azimuth viewing angle of the observations (Ulaby et al., 1981). At last, the surface is flat around Dome C, lower than $1\,\text{m}\,\text{km}^{-1}$ (Rémy et al., 1999), and thus the effect of azimuthal variations of the surface roughness on brightness temperature remains limited (Rémy and Parouty, 2009; Narvekar et al., 2010).

5 The surface roughness

The roughness of the snow surface has a direct influence on passive and active microwave observations (Rémy and Minster, 1991; Shuman et al., 1993; Flament and Rémy, 2012; Rémy et al., 2014; Adodo et al., 2018). Surface roughness ranges from ice sheet topography (100 km wavelength) and large dune fields (1 to 10 km wavelength) to small features on the surface, from millimetre to metre scale (hoar crystals and sastrugi, Shuman et al., 1993; Long and Drinkwater, 2000; Libois et al., 2014). Our

10 method requires a negligible effect of the surface roughness, and thus we discuss this assumption, first for active observations, and then for passive observations.

The slope of the large scale topography around Dome C are small enough, less than $1\,\text{m}\,\text{km}^{-1}$, to have a minor impact of the radar backscatter (Flament and Rémy, 2012). The pluri-annual trend can however be reduced considering a rough surface (Lacroix et al., 2008). Nevertheless, even with a lesser negative trend, ENVISAT and QuikSCAT observations confirm

15 the decrease of the surface snow density observed at Dome C by AMSR-E with completely independent data. QuickSCAT observations also suggest a slow evolution of the surface roughness.

Concerning passive microwave observations, as discussed in Champollion et al. (2013), the surface roughness influence is higher at vertical polarisation than at horizontal polarisation. The surface roughness tends to increase the polarisation ratio and reduces the retrieved density. As a result, the trend of the retrieved surface snow density can be reduced by an increase of the

20 surface roughness with time. The following reasons argue in favour of a small effect of the surface roughness even though we

can not conclude definitively: (1) Long and Drinkwater (2000) found a relatively low sensitivity of the polarisation ratio on surface roughness ; (2) the surface roughness is mainly governed by wind and, during the last decade, no clear wind evolution was found ; (3) most of the time, the lower is the frequency, the higher is the sensitivity of active microwave observations to surface roughness. This relationship is unclear for AMSR-E observations due to the difference of zenith viewing angle (Tsang,

5   1991; Liang et al., 2009). However, we should observe a frequency dependence of the polarisation ratio evolution if the surface roughness had evolved with time, at least for small scale roughness. Yet, the PR trends from AMSR-E are 0.00319 and 0.00326 at respectively 37 and 19 GHz which is compatible with thus a limited evolution of the small scale roughness. Concerning the large scale topography around Dome C, it has been previously discussed its minor impact on satellite observations.

The snow at depth

10   The snow below the top layer up to few metres depth influence the polarisation ratio through internal reflections. Changes in volume scattering (due to snow grains), caused by the evolution of snow deeper into the snowpack, certainly have a negligible direct effect on the retrieved density. However, snow evolution can change the penetration depth of the microwave emission and consequently change the number of snow–snow interfaces caused by abrupt changes in the snow density profile. Interface reflections are nearly independent of the wavelength according to Fresnel coefficients. The influence on ρ_{sat} of

15   snow changes deeper into the snowpack should thus be independent of the frequency. We consider an extreme case where the density stratification (either the number of layers with different dielectric constants into the snow, either the amplitude of the density variations) is always increasing with the decrease of surface snow density, keeping other snow parameters constant. The amount of internal reflections influences more the PR than the amplitude of the density difference between two layers. In addition, surface reflection is at least 4–5 times higher than internal reflections (Fig. 10). The case considered here (increase

20   of density stratification) leads to a decrease of the PR with time and thus an increase of the retrieved surface snow density. As a result, the trend of the retrieved density can be reduced by an increase of the snow density stratification. However, this effect remains probably small because changing the density of the second layer from 200 to 400 kg m^{-3} involves changes in the relationship between ρ_{sat} and PR_{37} lower than 20% (Fig. 10). Furthermore, changing the snow density of the third layer (figure not shown) results in an influence on PR slope less than 10%. As a result, decreasing the snow density of the second

25   layer by 10 kg m^{-3} (which is the trend of the retrieved density) has a weak influence on PR at 37 GHz. Modelling the evolution of the density profile is finally needed to definitively quantify its effect on the retrieved surface snow density. However, the sign of the trend will remain negative and the order of magnitude will probably remains the same.
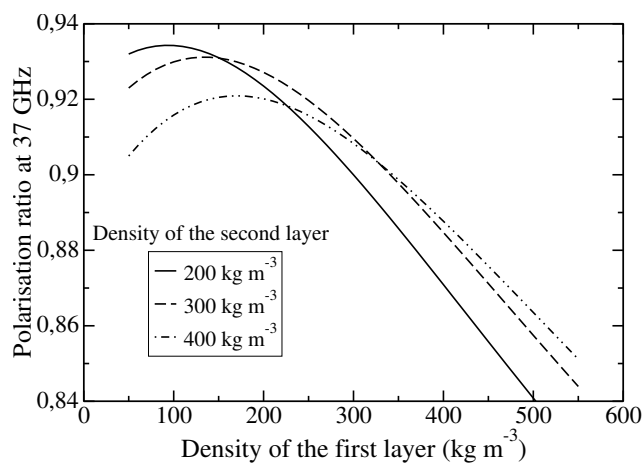
Figure 10. PR_{37} variations caused by changes in snow density of the top layer, for different snow densities of the second layer.

6 Conclusions

The snow density near the surface at Dome C on the East Antarctic Plateau has been estimated from passive microwave observations during nearly 10 years. The surface snow density retrieval method is based on the difference of Fresnel reflection coefficients between horizontally and vertically polarised brightness temperatures at the air–snow interface. The brightness

5   temperatures have been acquired by AMSR-E from 2002 to 2011. The DMRT-ML model has been used to compute the polarisation ratio (the ratio of horizontal on vertical brightness temperature) at the top-of-atmosphere using in situ profiles of snow parameters following Brucker et al. (2011). The comparison between modelled and observed brightness temperatures at 19 and 37 GHz, as well as the polarisation ratio sensitivity analyses to parameters of the top snow layer (3 centimetres thick), have permitted to highlight a relationship between the variations of the polarisation ratio at 37 GHz and the variations of the

10   snow density of the top layer.

    The main result of this study is the significant negative pluri-annual trend of surface snow density of about -13 kg m^{-3} yr^{-1}. We have not found a similar trend in the climatic conditions to explain such trend, even though it is likely that the cause is a change of atmospheric origin. This result has important consequence for surface mass balance estimation or regional climate modelling. Snow precipitation over the East Antarctic Plateau are expected to increase during the coming century (Krinner

15   et al., 2007). The time series also show an annual cycle as well as daily to weekly large density variations. The annual cycle could be linked to the amount of precipitation and the growing rate of the size of surface snow crystal size during the summer (Picard et al., 2012). The quick variations are certainly the results of interactions between the wind and the surface snow as well as the formation and disappearance of hoar crystals (Champollion et al., 2013; Libois et al., 2014).

    The retrieved time series of surface snow density has been compared to data available in the literature and to in situ mea-

20   surements. All data agreed together on the range of surface density values. Hoar crystals have a density between 125 and 178 kg m^{-3} and, when absent, surface snow density varies between 150 and 520 kg m^{-3} according to in situ measurements and between 136 and 508 kg m^{-3} for satellite retrieved density. In situ measurements show the same negative trend of about 10 kg m^{-3} yr^{-1} as the satellite observations. The pluri-annual decrease of surface snow density is also visible in active microwave observations (radar backscatter coefficient extracted from RA-2/ENVISAT and radar polarisation ratio calculated

25   from SeaWinds/QuikSCAT). As a result, SeaWinds/QuikSCAT observations show also a probable absence of evolution of the surface roughness. An overestimation of the decrease of surface snow density can however not be totally excluded, especially if surface roughness and/or density stratification in the snowpack increase in parallel with time.

    Thanks to the passive microwave observations which are all-weather daily and available for more than 30 years, the method can potentially be applied to the whole Antarctic ice sheet, after addressing the following issues: (1) include the surface

30   roughness, which can be more significant in other regions that at Dome C (Adodo et al., 2018), and the snow at depth in the retrieval method ; (2) include the regions where melt occurs (Picard et al., 2007) ; (3) inter-calibrate the different passive microwave satellites.

Competing interests. The authors declare that they have no conflict of interest.

Acknowledgements. AMSR-E, RA-2 and QuikSCAT data were respectively obtained from the National Snow and Ice Data Center (NSIDC) at University of Colorado, from the Center for Topographic studies of the Ocean and Hydrosphere (CTOH) supported by the European Space Agency (ESA) ENVISAT/RA-2 program and from the National Aeronautics and Space Administration (NASA) sponsored Scatterometer

5   Climate record Pathfinder (SCP) at Brigham Young University. We are very grateful to Ilhan Bourgeois, Sylvain Lafont and Sébastien Aubin to make snow density measurements at Dome C during the polar winter. Field measurements around Concordia Station were made possible by the joint French-Italian Concordia Program, which established and currently runs the permanent Concordia station at Dome C. We thus warmly thank the French polar institute (Institut Paul Emile Victor – IPEV) and the Italian polar program (Programma Nazionale di Ricerca in Antartide – PNRA). Finally, this work was supporting by the Programme National de Télédétection Spatiale (PNTS), the

10   IPEV programs (IPEV–CALVA and IPEV–GLACIOLOGIE) and the project MAPME (Monitoring of Antarctic Plateau by means of Multi-Frequency Microwave Emission) funded by PNRA.

References

Abdalati, W. and Steffen, K.: Accumulation and hoar effects on microwave emission on the Greenland ice sheet dry snow zones, J. Glaciol., 44, 523–531, http://cat.inist.fr/?aModele=afficheN&cpsidt=1710711, 1998.

Adodo, F. I., Remy, F., and Picard, G.: Seasonal variations of the backscattering coefficient measured by radar altimeters over the Antarctic Ice Sheet, The Cryosphere, 12, 1767–1778, https://doi.org/10.5194/tc-12-1767-2018, https://www.the-cryosphere.net/12/1767/2018/tc-12-1767-2018.pdf, 2018.

Alley, R. B., Bolzan, J. F., and Whillans, I. M.: Polar firn densification and grain growth, Ann. Glaciol., 3, 7–11, 1982.

Arnaud, L., Picard, G., Champollion, N., Domine, F., Gallet, J.-C., Lefebvre, E., Fily, M., and Barnola, J.-M.: Instruments and Methods. Measurement of vertical profiles of snow specific surface area with a 1 cm resolution using infrared reflectance: instrument description and validation, J. Glaciol., 57, 17–29, https://doi.org/10.3189/002214311795306664, http://www.ingentaconnect.com/content/igsoc/jog/2011/00000057/00000201/art00002?token=005b1f4873ea86f2dc4fdf87e2a46762c6b415d767667706a3a76452a673f7b2f267738703375686f4987f6f2dc, 2011.

Arthern, R. J., Winnebrenner, D. P., and Vaughan, D. G.: Antarctic snow accumulation mapped using polarization of 4.3-cm wavelength microwave emission, J. Geophys. Res., 111, 2156–2202, https://doi.org/10.1029/2004JD005667, http://dx.doi.org/10.1029/2004JD005667, 2006.

Arthern, R. J., Vaughan, D. G., Rankin, A. M., Mulvaney, R., and Thomas, E. R.: In situ measurements of Antarctic snow compaction compared with predictions of models, J. Geophys. Res., 115, https://doi.org/10.1029/2009JF001306, http://dx.doi.org/10.1029/2009JF001306, 2010.

Born, M. and Wolf, E.: Principles of Optics Electromagnetic. Theory of Propagation, Interference and Diffraction of Light., Cambridge University Press, http://www.amazon.com/Principles-Optics-Electromagnetic-Propagation-Interference/dp/0521642221, 1999.

Brucker, L., Picard, G., Arnaud, L., Barnola, J.-M., Schneebeli, M., Brunjail, H., Lefebvre, E., and Fily, M.: Modeling time series of microwave brightness temperature at Dome C, Antarctica, using vertically resolved snow temperature and microstructure measurements, J. Glaciol., 57, 171–182, https://doi.org/10.3189/002214311795306736, http://dx.doi.org/10.3189/002214311795306736, 2011.

Brucker, L., Dinnat, E., Picard, G., and Champollion, N.: Effect of Snow Surface Metamorphism on Aquarius L-Band Radiometer Observations at Dome C, Antarctica, IEEE T. Geosci. Remote, 52, 7408–7417, https://doi.org/10.1109/TGRS.2014.2312102, http://ieeexplore.ieee.org/xpl/articleDetails.jsp?arnumber=6805186, 2014.

Brun, E., Six, D., Picard, G., Vionnet, V., Arnaud, L., Bazile, E., Boone, A., Bouchard, A., Genthon, C., Guidard, V., Le Moigne, P., Rabier, F., and Seity, Y.: Snow/atmosphere coupled simulation at Dome C, Antarctica, J. Glaciol., 57, 721–736, https://doi.org/doi:10.3189/002214311797409794, http://www.ingentaconnect.com/content/igsoc/jog/2011/00000057/00000204/art00013, 2011.

Cavalieri, D., Markus, T., and Comiso, J.: AMSR-E/Aqua Daily L3 25 km Brightness Temperature & Sea Ice Concentration Polar Grids. Version 3, NASA National Snow and Ice Data Center Distributed Active Archive Center, https://doi.org/10.5067/AMSR-E/AE_SI25.003, http://nsidc.org/data/ae_si25/versions/3, 2014.

Champollion, N.: Évolution de la surface de neige sur le plateau Antarctique : observation in situ et satellite, Ph.D. thesis, Université de Grenoble Alpes, Grenoble, 2013.

Champollion, N., Picard, G., Arnaud, L., Lefebvre, E., and Fily, M.: Hoar crystal development and disappearance at Dome C, Antarctica: observation by near-infrared photography and passive microwave satellite, The Cryosphere, 7, 1247–1262, https://doi.org/10.5194/tc-7-1247-2013, http://www.the-cryosphere.net/7/1247/2013/tc-7-1247-2013.html, 2013.

Conger, S. M. and McClung, D. M.: Comparison of density cutters for snow profile observations, J. Glaciol., 55, 163–169, https://doi.org/10.3189/002214309788609038, http://www.ingentaconnect.com/content/igsoc/jog/2009/00000055/00000189/art00015, 2009.

Dee, D. P. and al.: The ERA-Interim reanalysis: configuration and performance of the data assimilation system, Q. J. Roy. Meteor. Soc., 137, 553–597, https://doi.org/10.1002/qj.828, http://onlinelibrary.wiley.com/doi/10.1002/qj.828/abstract, 2011.

Dominé, F., Salvatori, R., Legagneux, L., Salzano, R., Fily, M., and Casacchia, R.: Correlation between the specific surface area and the short wave infrared (SWIR) reflectance of snow, Cold Reg. Sci. Technol., 46, 60–68, https://doi.org/10.1016/j.coldregions.2006.06.002, http://www.sciencedirect.com/science/article/pii/S0165232X06000735, 2006.

Dominé, F., Albert, M., Huthwelker, T., Jacobi, H.-W., Kokhanovsky, A. A., Lehning, M., Picard, G., and Simpson, W. R.: Snow physics as relevant to snow photochemistry, Atmos. Chem. Phys., 8, 171–208, https://doi.org/10.5194/acp-8-171-2008, http://www.atmos-chem-phys.net/8/171/2008/acp-8-171-2008.html, 2008.

Dupont, F., Picard, G., Royer, A., Fily, M., Roy, A., Langlois, A., and Champollion, N.: Modeling the microwave emission of bubbly ice: Applications to blue ice and superimposed ice in the Antarctic and Arctic, IEEE T. Geosci. Remote, 2013.

Early, D. and Long, D.: Image Reconstruction and Enhanced Resolution Imaging from Irregular Samples, IEEE T. Geosci. Remote, 39, 291–302, https://doi.org/10.1109/36.905237, http://ieeexplore.ieee.org/xpls/abs_all.jsp?arnumber=905237&tag=1, 2001.

Eisen, O., Frezzotti, M., Genthon, C., Isaksson, E., Magand, O., Van den Broeke, M. R., Dixon, D. A., Ekaykin, A., Holmlund, P., Kameda, T., Karlöf, L., Kaspari, S., Lipenkov, V., Oerter, H., Takahashi, S., and Vaughan, D. G.: Ground-based measurements of spatial and temporal variability of snow accumulation in East Antarctica, Rev. Geophys., 46, 1–39, https://doi.org/10.1029/2006RG000218, http://www.agu.org/pubs/crossref/2008/2006RG000218.shtml, 2008.

Favier, V., Agosta, C., Genthon, C., Arnaud, L., Trouvillez, A., and Gallée, H.: Modeling the mass and surface heat budgets in a coastal blue ice area of Adelie Land, Antarctica, J. Geophys. Res., 116, https://doi.org/10.1029/2010JF001939, http://dx.doi.org/10.1029/2010JF001939, 2011.

Favier, V., Agosta, C., Parouty, S., Durand, G., Delaygue, G., Gallée, H., Drouet, A.-S., Trouvilliez, A., and Krinner, G.: An updated and quality controlled surface mass balance dataset for Antarctica, The Cryosphere Disuss., pp. 3667–3702, 2012.

Fettweis, X., Franco, B., Tedesco, M., van Angelen, J. H., Lenaerts, J. T. M., van den Broeke, M. R., and Gallée, H.: Estimating the Greenland ice sheet surface mass balance contribution to future sea level rise using the regional atmospheric climate model MAR, The Cryosphere, 7, 469–489, https://doi.org/10.5194/tc-7-469-2013, http://www.the-cryosphere.net/7/469/2013/, 2013.

Flament, T. and Rémy, F.: Dynamic thinning of Antarctic glaciers from along-track repeat radar altimetry, J. Glaciol., 58, 830–840, https://doi.org/doi:10.3189/2012JoG11J118, http://www.ingentaconnect.com/content/igsoc/jog/2012/00000058/00000211/art00002, 2012.

France, J. L., King, M. D., Frey, M. M., Erbland, J., Picard, G., Preunkert, S., MacArthur, A., and Savarino, J.: Snow optical properties at Dome C (Concordia), Antarctica; implications for snow emissions and snow chemistry of reactive nitrogen, Atmos. Chem. Phys., 11, 9787–9801, https://doi.org/10.5194/acp-11-9787-2011, http://www.atmos-chem-phys.net/11/9787/2011/, 2011.

Freville, H., Brun, E., Picard, G., Tatarinova, N., Arnaud, L., Lanconelli, C., Reijmer, C., and van den Broeke, M.: Using MODIS land surface temperatures and the Crocus snow model to understand the warm bias of ERA-Interim reanalyses at the surface in Antarctica, The Cryosphere, 8, 1361–1373, https://doi.org/10.5194/tc-8-1361-2014, https://www.the-cryosphere.net/8/1361/2014/, 2014.

Frezzotti, M., Pourchet, M., Flora, O., Gandolfi, S., Gay, M., Urbini, S., Vincent, C., Becagli, S., Gragnani, R., Proposito, M., Severi, M.,
5   Traversi, R., Udisti, R., and Fily, M.: Spatial and temporal variability of snow accumulation in East Antarctica from traverse data, J. Glaciol., 51, 113–124, https://doi.org/10.3189/172756505781829502, http://www.ingentaconnect.com/content/igsoc/jog/2005/00000051/00000172/art00011?token=004f11eaa5a666f3a7b6c5f40386f556b66523b3f2549264f655d375c6b6876305021a42be1ae0d, 2005.

Frezzotti, M., Scarchilli, C., Becagli, S., Proposito, M., and Urbini, S.: A synthesis of the Antarctic surface mass balance during the last 800 yr, The Cryosphere, 7, 303–319, https://doi.org/10.5194/tc-7-303-2013, http://www.the-cryosphere.net/7/303/2013/, 2013.

10   Fujita, S., Holmlund, P., Andersson, I., Brown, I., Enomoto, H., Fujii, Y., Fujita, K., Fukui, K., Furukawa, T., Hansson, M., Hara, K., Hoshina, Y., Igarashi, M., Iizuka, Y., Imura, S., Ingvander, S., Karlin, T., Motoyama, H., Nakazawa, F., Oerter, H., Sjöberg, L. E., Sugiyama, S., Surdyk, S., Ström, J., Uemura, R., and Wilhelms, F.: Spatial and temporal variability of snow accumulation rate on the East Antarctic ice divide between Dome Fuji and EPICA DML, The Cryosphere, 5, 1057–1081, https://doi.org/10.5194/tc-5-1057-2011, http://www.the-cryosphere.net/5/1057/2011/, 2011.

15   Gallet, J.-C., Dominé, F., Arnaud, L., Picard, G., and Savarino, J.: Vertical profile of the specific surface area and density of the snow at Dome C and on a transect to Dumont D'Urville, Antarctica – albedo calculations and comparison to remote sensing products, The Cryosphere, 5, 631–649, https://doi.org/10.5194/tc-5-631-2011, http://www.the-cryosphere.net/5/631/2011/tc-5-631-2011.html, 2011.

Gallet, J.-C., Dominé, F., Savarino, J., Dumont, M., and Brun, E.: The growth of sublimation crystals and surface hoar on the Antarctic plateau, The Cryosphere, 8, 1205–1215, https://doi.org/10.5194/tc-8-1205-2014, http://www.the-cryosphere.net/8/1205/2014/, 2014.

20   Genthon, C., Town, M. S., Six, D., Favier, V., Argentini, S., and Pellegrini, A.: Meteorological atmospheric boundary layer measurements and ECMWF analyses during summer at Dome C, Antarctica, J. Geophys. Res., 115, https://doi.org/10.1029/2009JD012741, http://www.agu.org/pubs/crossref/2010/2009JD012741.shtml, 2010.

Gergely, M., Schneebeli, M., and Roth, K.: First experiments to determine snow density from diffuse near-infrared transmittance, Cold Reg. Sci. Technol., 64, 81–86, https://doi.org/10.1016/j.coldregions.2010.06.005, http://www.sciencedirect.com/science/article/pii/
25   S0165232X10001308, 2010.

Groh, A., Ewert, H., Rosenau, R., Fagiolini, E., Gruber, C., Floricioiu, D., Abdel Jaber, W., Linow, S., Flechtner, F., Eineder, M., Dierking, W., and Dietrich, R.: Mass, Volume and Velocity of the Antarctic Ice Sheet: Present-Day Changes and Error Effects, Surv. Geophys., 35, 1481–1505, https://doi.org/10.1007/s10712-014-9286-y, http://link.springer.com/article/10.1007%2Fs10712-014-9286-y#, 2014.

Jin, Y.-Q.: Electromagnetic scattering modelling for quantitative remote sensing, World Scientific, http://www.worldscibooks.com/physics/
30   2253.html, 1994.

Krinner, G., Magand, O., Simmonds, I., Genthon, C., and Dufresne, J.-L.: Simulated Antarctic precipitation and surface mass balance at the end of the twentieth and twenty-first centuries, Clim. Dynam., 28, 215–230, https://doi.org/10.1007/s00382-006-0177-x, http://www.springerlink.com/content/h36074r475621h52/, 2007.

Lacroix, P., Dechambre, M., Legrésy, B., Blarel, F., and Rémy, F.: On the use of the dual-frequency ENVISAT altimeter to determine
35   snowpacks properties of the Antarctic ice sheet, Remote Sens. Environ., 112, 1712–1729, https://doi.org/10.1016/j.rse.2007.08.022, http://www.sciencedirect.com/science/article/pii/S0034425707004154, 2008.

Lacroix, P., Legrésy, B., Rémy, F., Blarel, F., Picard, G., and Brucker, L.: Rapid change of snow surface properties at Vostok, East Antarctica, revealed by altimetry and radiometry, Remote Sens. Environ., 113, 2633–2641, https://doi.org/doi:10.1016/j.rse.2009.07.019,

http://www.sciencedirect.com/science?_ob=MiamiImageURL&_cid=271745&_user=1531784&_pii=S0034425709002417&_check=
y&_origin=&_coverDate=15-Dec-2009&view=c&wchp=dGLbVlS-zSkWz&md5=51b4d429cbb444d256f35a4c207816c8/1-s2.
0-S0034425709002417-main.pdf, 2009.

Leduc-Leballeur, M., Picard, G., Mialon, A., Arnaud, L., Lefebre, F., Possenti, P., and Kerr, Y.: Modeling L-Band Brightness
Temperature at Dome C in Antarctica and Comparison With SMOS Observations, IEEE T. Geosci. Remote, 53, 4022–4032,
https://doi.org/10.1109/TGRS.2015.2388790, http://ieeexplore.ieee.org/stamp/stamp.jsp?arnumber=7031904, 2015.

Leduc-Leballeur, M., Picard, G., Macelloni, G., Arnaud, L., Brogioni, M., Mialon, A., and Kerr, Y.: Influence of snow surface properties on
L-band Brightness temperature at Dome C, Antarctica, Remote Sens. Environ., 199, 427–436, https://doi.org/10.1016/j.rse.2017.07.035,
https://www.sciencedirect.com/science/article/abs/pii/S0034425717303504, 2017.

Lenaerts, J. T. M. and van den Broeke, M. R.: Modeling drifting snow in Antarctica with a regional climate model: 2. Results, J. Geophys.
Res., 117, D05 109, https://doi.org/10.1029/2010JD015419, http://dx.doi.org/10.1029/2010JD015419, 2012.

Li, L., Gaiser, P., Albert, M. R., Long, D. G., and Twarog, E. M.: WindSat Passive Microwave Polarimetric Signatures of the Greenland Ice
Sheet, IEEE T. Geosci. Remote, 46, 2622–2631, https://doi.org/10.1109/TGRS.2008.917727, http://ieeexplore.ieee.org/xpls/abs_all.jsp?
arnumber=4579247, 2008.

Liang, D., Tse, K., Tan, Y., Tsang, L., and Kung Hau, D.: Scattering and Emission in Snow Based on QCA/DMRT and Numerical
Maxwell Model of 3Dimentional Simulations (NMM3D), pp. 197–202, MicroRad, IEEE Geoscience and Remote Sensing Society,
https://doi.org/10.1109/MICRAD.2006.1677088, http://ieeexplore.ieee.org/xpls/abs_all.jsp?arnumber=1677088&tag=1, 2006.

Liang, D., Xu, X., Tsang, L., Andreadis, K. M., and Josberger, E. G.: The Effects of Layers in Dry Snow on Its Passive Microwave Emissions
Using Dense Media Radiative Transfer Theory Based on the Quasicrystalline Approximation (QCA/DMRT), IEEE T. Geosci. Remote,
46, 3663–3671, https://doi.org/10.1109/TGRS.2008.922143, http://ieeexplore.ieee.org/xpls/abs_all.jsp?arnumber=4686016, 2008.

Liang, D., Xu, P., Tsang, L., Gui, Z., and Chen, K.: Electromagnetic scattering by rough surfaces with larges heights and slopes with
applications to microwave remote sensing of rough surface over layered media, Progress in Electromagnetics Research, 95, 199–218,
https://doi.org/10.2528/PIER09071413, http://www.jpier.org/PIER/pier.php?paper=09071413, 2009.

Libois, Q., Picard, G., France, J. L., Arnaud, L., Dumont, M., Carmagnola, C. M., and King, M. D.: Influence of grain shape on light penetra-
tion in snow, The Cryosphere, 7, 1803–1818, https://doi.org/10.5194/tc-7-1803-2013, 2013, http://www.the-cryosphere.net/7/1803/2013/
tc-7-1803-2013.html, 2013.

Libois, Q., Picard, G., Arnaud, L., Morin, S., and Brun, E.: Modeling the impact of snow drift on the decameter-scale variability of snow
properties on the Antarctic Plateau, J. Geophys. Res., 119, 11,662–11,681, https://doi.org/10.1002/2014JD022361, http://dx.doi.org/10.
1002/2014JD022361, 2014.

Libois, Q., Picard, G., Arnaud, L., Dumont, M., Lafaysse, M., Morin, S., and Lefebre, F.: Summertime evolution of snow specific surface
area close to the surface on the Antarctic Plateau, The Cryosphere, 9, 2383–2398, https://doi.org/10.5194/tc-9-2383-2015, http://www.
the-cryosphere.net/9/2383/2015/, 2015.

Long, D. and Daum, D.: Spatial Resolution Enhancement of SSM/I Data, IEEE T. Geosci. Remote, 36, 407–417, https://doi.org/0196-
2892(98)00550-6, http://www.mers.byu.edu/long/papers/TGARS1998Mar.pdf, 1998.

Long, D., Drinkwater, M., Holt, B., Saatchi, S., and Bertola, C.: Global Ice and Land Climate Studies Using Scatterometer Image Data, EOS,
Transaction of the American Geophysical Union, 82, 503–518, http://sites.agu.org/, 2001.

Long, D. G. and Drinkwater, M. R.: Azimuth Variation in Microwave Scatterometer and Radiometer Data Over Antarctica, IEEE T. Geosci.
Remote, 38, 1857–1870, https://doi.org/10.1109/36.851769, http://ieeexplore.ieee.org/stamp/stamp.jsp?tp=&arnumber=851769, 2000.

Lowe, H. and Picard, G.: Microwave scattering coefficient of snow in MEMLS and DMRT-ML revisited: the relevance of sticky hard spheres and tomography-based estimates of stickiness, The Cryosphere, 9, 2101–2117, https://doi.org/10.5194/tc-9-2101-2015, https://www.the-cryosphere.net/9/2101/2015/, 2015.

Macelloni, G., Brogioni, M., Pampaloni, P., and Cagnati, A.: Multifrequency Microwave Emission From the Dome-C Area on the East Antarctic Plateau: Temporal and Spatial Variability, IEEE T. Geosci. Remote, 45, 2029–2039, https://doi.org/10.1109/TGRS.2007.890805, http://ieeexplore.ieee.org/xpls/abs_all.jsp?arnumber=4261066, 2007.

Markus, T., Neumann, T. A., Martino, A., Abdalati, W., Brunt, K., Csatho, B., Farrell, S., Fricker, H., Gardner, A., Harding, D., Jasinski, M., Kwok, R., Magruder, L., Lubin, D., Luthcke, S., Morison, J., Nelson, R., Neuenschwander, A., Palm, S., Popescu, S., Shum, C. K., Schutz, B., Smith, B., Yang, Y., and Zwally, J.: The Ice, Cloud and land Elevation Satellite-2 (ICESat-2): Science requirements, concept, and implementation, Remote Sens. Environ., 190, 260–273, 2017.

Matzl, M. and Schneebeli, M.: Measuring specific surface area of snow by near-infrared photography, J. Glaciol., 52, 558–564, https://doi.org/10.3189/172756506781828412, http://www.ingentaconnect.com/content/igsoc/jog/2006/00000052/00000179/art00007?token=0050161659139b7e41225f4038762c6b675276782562706e576b34272c5f7b3d6d3f4e4b348f10c4, 2006.

Mätzler, C., Aebischer, H., and Schanda, E.: Microwave dielectric properties of surface snow, Journal of Oceanic Engineering, OE-9, 366–371, https://doi.org/10.1109/JOE.1984.1145644, http://ieeexplore.ieee.org/xpls/abs_all.jsp?arnumber=1145644, 1984.

McMillan, M., Shepherd, A., Sundal, A., Briggs, K., Muir, A., Ridout, A., Hogg, A., and Wingham, D.: Increased ice losses from Antarctica detected by CryoSat-2, Geophys. Res. Lett., 41, 3899–3905, https://doi.org/10.1002/2014GL060111, http://dx.doi.org/10.1002/2014GL060111, 2014.

Mittal, S. K., Singh, M., and Garg, P. K.: Development of an instrument to measure density and moisture content of snow, Journal of Scientific & Industrial Research, 68, 188–191, http://nopr.niscair.res.in/handle/123456789/3169, 2009.

Narvekar, P. S., Heygster, G., Jackson, T. J., Bindlish, R., Macelloni, G., and Justus, N.: Passive Polarimetric Microwave Signatures Observed Over Antarctica, IEEE T. Geosci. Remote, 48, 1059–1075, https://doi.org/10.1109/TGRS.2009.2032295, http://ieeexplore.ieee.org/stamp/stamp.jsp?tp=&arnumber=5345832, 2010.

Palerme, C., Kay, J. E., Genthon, C., L'Ecuyer, T., Wood, N. B., and Claud, C.: How much snow falls on the Antarctic ice sheet?, The Cryosphere, 8, 1577–1587, https://doi.org/10.5194/tc-8-1577-2014, http://www.the-cryosphere.net/8/1577/2014/, 2014.

Picard, G., Fily, M., and Gallée, H.: Surface melting derived from microwave radiometers: a climatic indicator of Antarctica, Ann. Glaciol., 46, 29–34, https://doi.org/10.3189/172756407782871684, http://dx.doi.org/10.3189/172756407782871684, 2007.

Picard, G., Brucker, L., Fily, M., Gallée, H., and Krinner, G.: Modeling time series of microwave brightness temperature in Antarctica, J. Glaciol., 55, 537–551, https://doi.org/10.3189/002214309788816678, http://www.ingentaconnect.com/content/igsoc/jog/2009/00000055/00000191/art00016?token=004510f141333c4a2f7a736a6f2c31465d7d28463e4f6d62222c227e3725303329762, 2009.

Picard, G., Domine, F., Krinner, G., Arnaud, L., and Lefebvre, E.: Inhibition of the positive snow-albedo feedback by precipitation in interior Antarctica, Nat. Clim. Change, 2, https://doi.org/10.1038/nclimate1590, http://www.nature.com/nclimate/journal/vaop/ncurrent/full/nclimate1590.html, 2012.

Picard, G., Brucker, L., Roy, A., Dupont, F., Fily, M., Royer, A., and Harlow, C.: Simulation of the microwave emission of multi-layered snowpacks using the Dense Media Radiative Transfer theory: the DMRT-ML model, Geosci. Model Dev., 6, 1061–1078, https://doi.org/10.5194/gmd-6-1061-2013, http://www.geosci-model-dev.net/6/1061/2013/gmd-6-1061-2013.html, 2013.

Picard, G., Royer, A., Arnaud, L., and Fily, M.: Influence of meter-scale wind-formed features on the variability of the microwave brightness temperature around Dome C in Antarctica, The Cryosphere, 8, 1105–1119, https://doi.org/10.5194/tc-8-1105-2014, http://www.the-cryosphere.net/8/1105/2014/, 2014.

Proksch, M., Rutter, N., Fierz, C., and Schneebeli, M.: Intercomparison of snow density measurements: bias, precision and spatial resolution, The Cryosphere, 10, 371–384, https://doi.org/10.5194/tc-10-371-2016, https://doi.org/10.5194/tc-10-371-2016, 2016.

Rémy, F. and Minster, J.: A comparison between active and passive microwave measurements of the Antarctic ice sheet and their association with the surface katabatic winds, J. Glaciol., 37, 3–10, 1991.

Rémy, F. and Parouty, S.: Antarctic Ice Sheet and Radar Altimetry: A Review, Radio Sci., 1, 1212–1239, https://doi.org/10.3390/rs1041212, http://www.mdpi.com/2072-4292/1/4/1212/, 2009.

Rémy, F., Shaeffer, P., and Legrésy, B.: Ice flow physical processes derived from the ERS-1 high-resolution map of the Antarctica and Greenland ice sheets, Geophys. J. Int., 139, 645–656, https://doi.org/10.1046/j.1365-246x.1999.00964.x, http://onlinelibrary.wiley.com/doi/10.1046/j.1365-246x.1999.00964.x/pdf, 1999.

Rémy, F., Flament, T., Michel, A., and Verron, J.: Ice sheet survey over Antarctica with satellite altimetry: ERS-2, EnviSat, SARAL/AltiKa, the key importance of continuous observations along the same repeat orbit, Int. J. Remote Sens., 35, 5497–5512, https://doi.org/10.1080/01431161.2014?926419, 2014.

Rosenkranz, P.: Rough-sea microwave emissivities measured with the SSM/I, IEEE T. Geosci. Remote, 30, 1081–1085, https://doi.org/10.1109/36.175345, http://ieeexplore.ieee.org/xpls/abs_all.jsp?arnumber=175345&tag=1, 1992.

Roy, A., Picard, G., Royer, A., Montpetit, B., Dupont, F., Langlois, A., Derksen, C., and Champollion, N.: Brightness temperature simulations of the Canadian seasonal snowpack driven by measurements of snow specific surface area, IEEE T. Geosci. Remote, 2012.

Schwank, M. and Naderpour, R.: Snow Density and Ground Permittivity Retrieved from L-Band Radiometry: Melting Effects, Radio Sci., 10, https://doi.org/10.3390/rs10020354, 2018.

Shuman, C. A. and Alley, R. B.: Spatial and temporal characterization of hoar formation in central Greenland using SSM/I brightness temperatures, Geophys. Res. Lett., 20, 2643–2646, https://doi.org/10.1029/93GL02810, http://www.agu.org/pubs/crossref/1993/93GL02810.shtml, 1993.

Shuman, C. A., Alley, R. B., and Anandakrishnan, S.: Characterization of a hoar-development episode using SSM/I brightness temperatures in the vicinity of GISP2 site, Greenland, Ann. Glaciol., 17, 183–188, https://doi.org/01/1993; 17:183-188, http://www.igsoc.org/annals.old/17/igs_annals_vol17_year1993_pg183-188.pdf, 1993.

Sommer, C. G., Wever, N., Fierz, C., and Lehning, M.: Investigation of a wind-packing event in Queen Maud Land, Antarctica, The Cryosphere, 12, 2923–2939, 2018.

Spencer, M., Wu, C., and Long, D.: Improved Resolution Backscatter Measurement with the SeaWinds Pencil-Beam Scatterometer, IEEE T. Geosci. Remote, 38, 89–104, https://doi.org/0196-2892(00)00017-6, http://www.et.byu.edu/~long/papers/TGARS2000Jan.pdf, 2000.

Surdyk, S.: Using microwave brightness temperature to detect short-term surface air temperature changes in Antarctica: An analytical approach, Remote Sens. Environ., 80, 256–271, https://doi.org/10.1016/S0034-4257(01)00308-X, http://www.sciencedirect.com/science/article/pii/S003442570100308X, 2002a.

Surdyk, S.: Low microwave brightness temperatures in central Antarctica: observed features and implications, Ann. Glaciol., 34, 134–140, https://doi.org/10.3189/172756402781817464, http://www.ingentaconnect.com/content/igsoc/agl/2002/00000034/00000001/art00021?token=004913a2ed9573d2570257045232b2f2a31254d313a677c4e7547543c7e386f642f466f8c, 2002b.

Tedesco, M.: Remote Sensing of the Cryosphere, Cryosphere Science Series, John Wiley & Sons, Ltd, https://doi.org/10.1002/9781118368909, http://onlinelibrary.wiley.com/book/10.1002/9781118368909, 2015.

Tsang, L.: Polarimetic Passive Microwave Remote Sensing of Random Discrete Scatterers and Rough Surfaces, Journal of Electromagnetic Waves and Applications, 5, 41–57, https://doi.org/10.1163/156939391X00464, http://www.tandfonline.com/doi/abs/10.1163/156939391X00464?journalCode=tewa20, 1991.

Tsang, L., Chen, C.-T., Chang, A. T., Guo, J., and Ding, K.-H.: Dense media radiative transfer theory based on quasicrystalline approximation with application to passive microwave remote sensing of snow, Radio Sci., 35, 741–749, https://doi.org/10.1029/1999RS002270, http://www.agu.org/pubs/crossref/2000/1999RS002270.shtml, 2000a.

Tsang, L., Kong, J., and Ding, K.: Scattering of Electromagnetic Waves, Vol. 1: Theory and Applications, vol. 1, Wiley Interscience, 2000b.

Tsang, L., Xu, P., and Chen, K. S.: Third and fourth stokes parameters in polarimetric passive microwave remote sensing of rough surfaces over layered media, Microwave and Optical Technology Letters, 50, 3063–3069, https://doi.org/10.1002/mop.23892, http://onlinelibrary.wiley.com/doi/10.1002/mop.23892/abstract, 2008.

Ulaby, F. T., Moore, R. K., and Fung, A. K.: Microwave Remote Sensing: Active and Passive, Vol. I: Fundamentals and Radiometry, vol. I, Artech House Publishers, Massachusetts, http://www.amazon.com/Microwave-Remote-Sensing-Fundamentals-Radiometry/dp/0890061904, 1981.

Ulaby, F. T., Moore, R. K., and Fung, A. K.: Microwave Remote Sensing: Active and Passive, Vol. II: Radar Remote Sensing and Surface Scattering and Emission Theory, vol. II, Artech House Publishers, Massachusetts, http://www.amazon.com/Microwave-Remote-Sensing-Scattering-Emission/dp/0890061912, 1982.

Verfaillie, D., Fily, M., Le Meur, E., Magand, O., Jourdain, B., Arnaud, L., and Favier, V.: Snow accumulation variability derived from radar and firn core data along a 600 km transect in Adelie Land, East Antarctic plateau, The Cryosphere, pp. 1345–1358, https://doi.org/10.5194/tc-6-1345-2012, http://www.the-cryosphere.net/6/1345/2012/tc-6-1345-2012.html, 2012.

Vernon, C. L., Bamber, J. L., Box, J. E., van den Broeke, M. R., Fettweis, X., Hanna, E., and Huybrechts, P.: Surface mass balance model intercomparison for the Greenland ice sheet, The Cryosphere, 7, 599–614, https://doi.org/10.5194/tc-7-599-2013, http://www.the-cryosphere.net/7/599/2013/, 2013.

Walden, V. P., Warren, S. G., and Tuttle, E.: Atmospheric Ice Crystals over the Antarctic Plateau in Winter, J. Appl. Meteorol., 42, 1391–1405, https://doi.org/10.1175/1520-0450(2003)042<1391:AICOTA>2.0.CO;2, http://dx.doi.org/10.1175/1520-0450(2003)042%3C1391:AICOTA%3E2.0.CO;2, 2003.

Warren, S. G. and Brandt, R. E.: Optical constants of ice from the ultraviolet to the microwave: A revised compilation, J. Geophys. Res., 113, https://doi.org/10.1029/2007JD009744, http://www.agu.org/pubs/crossref/2008/2007JD009744.shtml, 2008.

Zwaaftink, C. D., Cagnati, A., Crepaz, A., Fierz, C., Macelloni, G., Valt, M., and Lehning, M.: Event-driven deposition of snow on the Antarctic Plateau: analyzing field measurement with SNOWPACK, The Cryosphere, 7, 333–347, 2013.